Facies variations in response to tectonic evolution, climate and sea-level changes since the Late Cretaceous in Wuhu region, Eastern China

Ting Wang[1], Longjiang Mao[1]*, Chunhui Zou[2],
Huichuan You[3] and Duowen Mo[4]

[1]School of Marine Science, Nanjing University of Information Science and Technology, Nanjing,
China, [2]Institute of the History of Science and Technology, Nanjing University of Information
Science and Technology, Nanjing, China, [3]Institute of Geophysics, China Earthquake
Administration, Beijing, China, [4]College of Urban and Environmental Science, Peking University,
Beijing, China

Eastern China has a complex environmental dynamics system in the western Pacific tectonic domain, and the study of its sedimentary records controlled by tectonic movements is distinctly significant for exploring sea-land interactions, global climate change and sea level fluctuations. A reliable OSL (Optically Stimulated Luminescence) chronostratigraphic framework was established based on a systematic investigation of the stratigraphic lithology of the boreholes in Wuhu area, Eastern China, and the depositional environment since the Late Cretaceous was reconstructed by multiple environmental proxies. Significant regional changes in sedimentary activity since the Mesozoic indicate that the Yanshan movement and the Neotectonic movement controlled the evolution of sedimentary basins and fracture tectonics in the study area and influenced the paleo-geographic environment and sedimentary patterns in a regional geotectonic context. Since the Middle Pleistocene, the temperature and sea level trends were split into six stages, four of which (MIS 6, 4, 3 and 2) can be categorized as periods of decline, with MIS 1 being a period of significant increase. The other phase (MIS 5) was characterized by violent fluctuations in climate and sea level, with periods of increase in MIS 5a, 5c and 5e and decrease in MIS 5b and 5d. Sedimentary process in eastern China are mainly controlled by regional geotectonic activity, and the specific evolution of the depositional environment is also influenced by the combined effects of regional climate and sea level.

KEYWORDS

tectonic evolution, climate change, sea level, the Late Cretaceous to Holocene, Wuhu riverine area, Eastern China

Introduction

The river-ocean interaction area is a strong ocean-land-atmosphere interaction zone. Under the impacts on extreme climate events, sea-level fluctuation and regional crustal movements, sediments record a vast amount of information on natural environmental evolution and are therefore very sensitive to global climate and paleo-environmental changes (Wang et al., 2007; Wang and Ji, 2011; Yao, 2014; Liu et al., 2010; Ghandour et al., 2021). The study of climate-sea level change and local sedimentary response of land-ocean systems has become a crucial issue in the evolution of the global environment, and is vital to address current changes in anthropogenic climate and geospatial patterns (Feist et al., 2019; Singh and Sinha, 2019; Yang et al., 2022). For example, studies of the geological setting of Deedsville Bay, the Bahamas, and the Garigliano Plain have suggested that regional environmental evolution is mostly controlled by climate extremes, changes in water regimes, and sea level fluctuations (Aiello et al., 2021; Kindler and Hearty, 2022; Noorian et al., 2022). Understanding past environmental evolution is imperative for exploring global climate-sea level fluctuations and the distribution of geological resources over long timescales.

The Wuhu area is located in the northern margin of lower Yangtze plate, with a complex structural system, and was influenced by the collisional subduction between the Transpacific plate and Eurasian plate during the Mesozoic-Cenozoic period, with obvious signs of fracture zone and volcanic activity (Wang et al., 2007; Zhu et al., 2012; Yang et al., 2016; Qiu et al., 2018; Wu et al., 2020). Previous studies have shown that tectonic processes are one of the fundamental factors affecting the supply of material sources in river basins (Li and Zhang, 2003; Henderson et al., 2010; Liu, 2018; Lal et al., 2019). For example, the lower Yangtze River has been strongly affected by the Indo-China movement (crustal movements occurring from Triassic to Early Jurassic) since the Mesozoic by large-scale sea retreat events, which developed extensive terrestrial sediments in Wuhu, Tongling and Fanchang area (Zhou and Chen, 1992; Chen, 2020). Moreover, the Yanshan movement (extensive crustal movement from Jurassic to Cretaceous in China) was caused by the westward collisional subduction of the paleo-Pacific plate and Asia-European plate resulting in extensive magmatic intrusion in eastern China (Yan et al., 2000; Grant et al., 2014). Changes in climate and sea level have intrinsic effects on the sediment cycle, including changes in sedimentation rates, water regime size, and datum. Vegetation condition, weathering intensity, sediment composition, and riverine sediment transport can change significantly under the influence of climate fluctuations during different geological and historical periods (Bell, 1975; Wang, 2008; Cui, 2017). Therefore, paleoclimate proxy features such as sediment grain size, magnetic susceptibility and chromaticity have been used to reflect and reconstruct the paleo-environment (Xiong et al.,

1998; Yan et al., 2000; Bouchez et al., 2011; Aiello et al., 2021). To date, several geological and sedimentological investigations have been carried out in the Wuhu riverine area, most of which focus on Quaternary river and lake sediments and stratigraphic lithology, while there is a lack of in-depth studies on the differences of stratigraphic depositional sequences on both sides of the riverine hedge zone under different tectonic environments and the evolutionary history of the sedimentary environment since the Late Cretaceous in the lower reaches of the Yangtze River.

To reveal the evolutionary history of the sedimentary environment in eastern China since the Late Cretaceous, we have investigated and analyzed the sedimentary sequence, lithological characteristics of the sedimentary strata, hydrodynamic conditions and redox environment in the region based on the establishment of a feasible chronological framework. Our study aims to comprehensively analyze the sedimentary face characteristics of borehole cores in Wuhu and its surrounding areas and to reconstruct the complete history of sedimentary environment evolution based on the specific local paleogeographic environment and crustal movement, as well as relative sea level fluctuations and climate evolution records. This detailed analysis may also be more helpful in understanding the major geological events that have occurred since the Late Cretaceous, which have resulted in significant changes in the geographic pattern of eastern China. Therefore, our objectives are to: (1) to acquire the evolution records of the sedimentary environment in the lower reaches of the Yangtze River since the Late Cretaceous; (2) to explore the regional tectonic movements and paleo-geographical patterns in eastern China since the Mesozoic; (3) to reveal the sedimentary processes response to regional and global climate and sea level changes.

Regional setting

Wuhu area is located in the plain area of middle and lower reaches of Yangtze River, with a subtropical humid monsoon climate, annual average temperature of 17-18°C, abundant light and rainfall (WLRCC, 1993; Fang, 2005; Su, 2007). Due to the influence of plate motion, folded tectonic deformation and extensional tectonic deformation activities in eastern China since the Mesozoic, the Wuhu region has a complex tectonic environment. The Wuhu region is at the northern margin of the Lower Yangzi plate, adjacent to the Tanlu fault zone, the Dabie orogenic belt and the North China plate (Figure 1), and is strongly influenced by the riverine ramp zone (Xu and Gao, 2015; Xu et al., 2018). Eastern China is located between the Eurasian plate and Pacific plate, in the Circum Pacific tectonic domain, which is mainly composed of the North China Craton, the South China Block (consisting of the Cathaysia Block and the Yangtze Craton), large orogenic belts (such as the Jiangnan
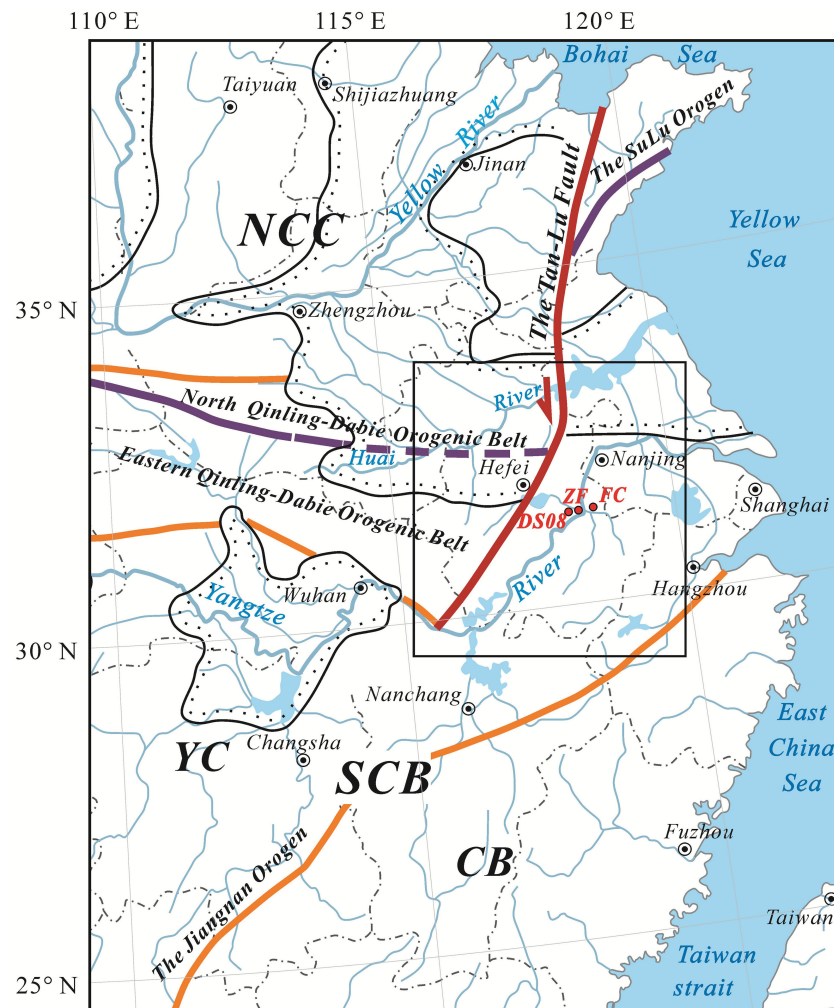
FIGURE 1
The important orogenic belt in eastern China, the geographical location of the study area, and the locations of boreholes ZF, FC and DS08; NCC is the North China Craton, SCB is the South China Block, YC is the Yangtze Craton, and CB is the Cathaysia Block.

orogenic belt, the Qinling-Dabie orogenic belt, and the Sulu orogenic belt), and important hydrocarbon-bearing basins (Ren et al., 2002; Zheng et al., 2013; Xu et al., 2021). Since the late Mesozoic, tight westward subduction of the paleo-Pacific plate has led to extensive and extreme tectonic activity in eastern China, such as regional extension of the continental margin, intraplate tectonic deformation, magmatic activity, and the formation of the Craton Basin, resulting in the present-day regional solid topographic contrast and extensive fracture zones (Liu, 2007; Zheng et al., 2013. Xu et al., 2021; Noorian et al., 2022). Among them, the Tanlu fault is the most important impact-slip fault in East Asia, and its Mesozoic impact-slip activity divides the Dabie Mountain-Sulu orogenic belt into the western and eastern segments, affecting regional crustal stability (Zheng et al., 2013; Zheng, 2019).

Material and methods

Field investigation

In November 2020, two boreholes were drilled on both sides in Wuhu riverine area to obtain sediments, using the rotary drilling method, where significant chronostratigraphic development and sedimentary features, and named the ZF (31° 19′56″N, 118°18′45″E; depth: 49.9 m) and FC (31°22′41″N, 118° 26′56″E; depth: 83.4 m) boreholes (Figure 1). Both boreholes were characterized for sediment texture, color and sedimentary structure, and sedimentary environmental and chronological samples were collected. Environmental samples were collected at intervals of 1 to 1.5 m according to lithologic characteristics, and 1 to 2 OSL samples were taken from each layer. A total of

225 environmental samples and 7 OSL samples were obtained from the ZF borehole, and 367 environmental samples and 8 OSL samples were collected from the FC borehole.

OSL dating

In order to establish a reliable chrono-stratigraphy, 20 cm lengths of core sediment were selected for dating from homogeneous sediments from different stratigraphic units or from above and below close to the stratigraphic interface, which were deposited *in situ* without significant interference (Table 1; Aitken, 1998). Samples were collected from sealed PVC tubes with quickly and immediately wrapped in aluminum foil, and placed in black sealed light-proof bags. After removing the outer 2 to 4 cm of the sample and retaining only the undisturbed dense central portion, all samples were added 10% HCl and 38% H_2O_2 to remove carbonates and organic matter. Following the precipitation separation of 4-11 μm particles according to Stoker's law (Porat et al., 1999; Wintle, 2008; Bowman et al., 2004), the feldspar in the particles was dissolved with 35% hexafluorosilicic acid (H_2SiF_6) and treated with 10% hydrochloric acid to remove acid-soluble fluoride precipitates (Lai, 2010; Xu et al., 2020). The ethanol-purified quartz grains were then measured on a Risø TL/OSL-DA-15 optical release tomograph. OSL dating of all samples was carried out in the laboratory of the Institute of Geographical Sciences of the Henan Academy of Sciences.

Grain size analysis

In the laboratory analysis, carbonates and organic matter in the sediment were first removed by adding HCl (25%) and H_2O_2

(10%) successively to the sample following the chemical pretreatment procedure described by Konert and Vandenberghe (1977) and left to stand for 24 h, respectively. A 0.5 mol/L sodium hexametaphosphate solution was added to soak the samples for 24 h, and the samples were gently stirred every eighth to disperse completely. All samples were then put into a laser sample jar in order to be dispersed uniformly again by ultrasonic shaking and high-speed centrifugation. We measured samples up to 2 mm by using a Malvern Mastersizer-2000 laser grain sizer, and the repeatability and stability of the instrument were evaluated using the Malvern quality standard (QA3002 glass beads). The basic grain size classification of the sediments mainly followed the Udden-Wentworth classification (Udden, 1914; Wentworth, 1922). The analytical errors of all the above experiments were <5% at 95% confidence level. Afterward, the mean grain size (M_Z), sorting coefficient (S_O), skewness (S_K), and kurtosis (KG) were calculated for each sample according to the formula of Folk and Ward (1957). To reduce errors, we used a weighting method to obtain the average of the grain size index values for all samples at each sampling site, which was subsequently calculated using GRADISTAT software version 8. In addition, weakly cemented and loose sediment samples above 2 mm were sieved on a shaker for about 10-15 min using sieve analysis and then graded and weighed, which should be accurate to 0.01 g, or 0.001 g if the graded amount is less than 1.00 g (Folk, 1974; Liu, 1981; Yuan et al., 2019).

Magnetization analysis

The magnetization of the sediments was measured indoors using an MS-2 magnetometer manufactured by Bartington instruments, UK. All samples were dried in a drying oven,

TABLE 1 The optical luminescence (OSL) dating results of the ZF and FC boreholes in Wuhu.

Lab N.	Sample N.	Depth(m)	U/ppm	Th/ppm	K/%	Q-De(Gy)	w.c (%)	Q-Dose rate	Age (ka)
L769	ZF-001	8.35-8.50	1.98 ± 0.04356	12.2 ± 0.4758	1.79 ± 0.004296	8.31 ± 0.26	22.17	3.062 ± 0.137	2.714 ± 0.148
L770	ZF-003	12.75-12.85	3.68 ± 0.0184	24.5 ± 0.7105	1.83 ± 0.004941	7.41 ± 0.07	36.34	3.952 ± 0.23	1.875 ± 0.111
L771	ZF-005	21.50-21.60	1.86 ± 0.02046	8.79 ± 0.21096	2.13 ± 0.006603	20.53 ± 0.96	15.21	3.216 ± 0.115	6.385 ± 0.376
L772	ZF-007	29.60-29.70	2.38 ± 0.03332	14.1 ± 0.1269	1.94 ± 0.012998	15.60 ± 0.57	17.99	3.533 ± 0.165	4.416 ± 0.262
L773	ZF-009	34.20-34.30	1.69 ± 0.0272	9.84 ± 0.26568	1.96 ± 0.010584	12.21 ± 0.32	26.76	2.762 ± 0.106	4.42 ± 0.205
L774	ZF-011	38.40-38.50	1.84 ± 0.00736	11.7 ± 0.1872	1.82 ± 0.00182	8.55 ± 0.21	28.96	2.769 ± 0.119	3.088 ± 0.153
L775	ZF-013	44.80-44.90	1.45 ± 0.02465	7.43 ± 0.21547	2.51 ± 0.007781	98.65 ± 2.47	13.65	3.362 ± 0.097	29.344 ± 1.12
L756	FC-001	7.60-7.90	2.65 ± 0.037	15.4 ± 0.216	1.55 ± 0.003	20.92 ± 0.47	24.13	3.224 ± 0.169	6.448 ± 0.366
L757	FC-003	14.20-14.30	2.63 ± 0.04	15.6 ± 0.266	1.54 ± 0.002	46.90 ± 0.97	22.89	3.247 ± 0.173	14.444 ± 0.825
L758	FC-005	19.57-19.67	3.18 ± 0.009	16.4 ± 0.262	1.65 ± 0.003	29.03 ± 0.30	34.20	3.197 ± 0.169	9.08 ± 0.488
L759	FC-006	23.02-23.14	2.64 ± 0.063	14.5 ± 0.276	1.33 ± 0.012	38.13 ± 0.30	18.14	3.113 ± 0.174	12.249 ± 0.692
L760	FC-008	27.90-28.10	3 ± 0.075	18.4 ± 0.46	1.9 ± 0.006	237.73 ± 9.50	15.76	4.126 ± 0.22	57.623 ± 3.843
L761	FC-010	32.20-32.30	4.68 ± 0.145	19.4 ± 0.155	1.84 ± 0.004	394.87 ± 3.82	17.56	4.561 ± 0.262	86.584 ± 5.037
L762	FC-012	36.78-36.88	2.74 ± 0.107	18.1 ± 0.399	1.83 ± 0.128	461.91 ± 9.28	21.10	3.760 ± 0.217	122.856 ± 7.515
L764	FC-014	45.10-45.20	2.33 ± 0.047	6.84 ± 0.28	0.9 ± 0.002	300.06 ± 32.98	6.439	2.281 ± 0.129	131.552 ± 16.257

ground without damaging the natural grain, and soil samples were collected in 1 cm^3 non-magnetic cassettes and weighed before being tested with an MS-2 magnetization meter. The instrument's frequency should be set to 4.7 kHz for high frequencies and 0.47 kHz for low frequencies, and SI and 0.1 for unit and measurement steps, respectively. During the test, the background value of the instrument was measured once, then the magnetization of the sample was measured twice, and the background value of the instrument was measured once again after the sample was finally removed. All samples were measured three times, and the average value was taken as the final measurement result. After measuring the volumetric magnetic induction and density of the samples, the low-frequency magnetic induction (χlf), high-frequency magnetic induction (χhf) frequencies, and magnetic induction (χfd) were calculated. The calculation formula is $\chi fd=(\chi lf-\chi hf)/\chi lf\times100\%$.

Chroma analysis

The samples were naturally and uniformly air-dried in the laboratory and pounded and ground to a fineness of approximately 200 nm or less without damaging the sediment grain structure to minimize the effect of soil moisture and soil grain size on soil color. The experimental conditions, especially the background light source, were kept constant throughout the test. The data were measured using a Minolta CM-2002 spectrophotometer according to the CIELAB colorimetric system. The samples were calibrated on a standard calibration white plate of a K-Minolta CR-400 colorimeter made in Japan, flattened without wrinkling. The same sample was measured three times in different areas, and the average values of L* (brightness), a* (redness), and b* (yellowness) were recorded so that the error was less than 0.07.

Results

Lithology description

Through detailed observation and study of the sedimentary strata of the ZF and FC boreholes with detailed lithology, sedimentary structure, structure, and sedimentary cycle, it is found that the sedimentary facies of the ZF and FC boreholes are significantly different (Tables 2, 3; Figure 2). As shown in Table 2, the ZF borehole is mainly composed of sand-dominated fluvial deposits, with a small proportion of clay and silty clay, showing a typical lower coarse and upper fine binary structure. The bottom of the borehole (depth 49.9 to 48.75 m) is mainly weathering products of the amphibolite, including fragments of grey-purple mudstone encased in bedrock formed by total weathering and rock fragments formed by strong weathering (Table 2). Above the bedrock, between 48.75-47.1m depth, the stratigraphy is dominated by a greenish grey muddy boulder-gravel layer, which is river-lake facies (Table 2). While the ZF borehole is characterized by a large amount of yellowish-grey medium to coarse sand and gravel in 47.1 to 42.5 m depth, which belongs to alluvial fan subphase with a clear erosional boundary with its lower strata. Most of the ZF borehole sediments consist of stratigraphic silt, fine sand, and medium-fine sand (depth 42.5 to 0 m), which are belonged to fluvial facies (Table 2), and there are multiple coarse to fine grain size sedimentation cycles from the base to the top (Figure 2).

The lithology and sedimentary environment of the strata in the FC borehole are sophisticated and have shown significant segmentation with depth (Table 3; Figure 2). The lower stratigraphy is dominated by moderately weathered bedrock, including brick-red mudstone and grey gypsiferous mudstone (depth 83.4 to 74.45 m) and gravelly brick-red siltstone (depth 74.45 to 60.5 m), which were deposited in river-lake facies

TABLE 2 The stratigraphic description and sedimentary facies of the ZF borehole in Wuhu.

Depth of strata / m	Stratigraphic Description	Sedimentary facies
0-14.50	Grey, greyish-black silty and fine sand with many clay belts, with abundant mica; some soil-forming processes at the top, containing many plant roots.	River floodplain facies
14.50-32.50	Dark grey, gray-black fine and medium-fine sand, gradually becoming coarser from bottom to top, with a few coarse sand and gravels.	Alluvial facies
32.50-42.50	Gray-black fine and medium-fine sand, gradually becoming finer from bottom to top, occasional brownish clay belts and plant roots aggregate; medium to coarse sand at the bottom, with a few yellow gravels.	Alluvial-diluvial facies、River floodplain facies
42.50-47.10	Yellowish grey, dark grey medium to coarse sand and gravel with medium to good roundness of the gravel.	Alluvial fan subphase
47.10-48.75	Calcareous conglomeratic mudstone with many well-rounded pebbles in the upper part and many greenish silt clumps and gray-white clayey silt belts in the lower part.	River-lake facies
48.75-49.90	Glaucous diorite-porphyrite weathering residues, the upper part is full weathered with a large number of dark green bedrock residue grains wrapped in grey-purple mudstone; the lower part is strongly weathered with massive grey-green weathering residues.	Weathering residues of bedrock

TABLE 3 The stratigraphic description and sedimentary facies of the FC borehole in Wuhu.

Depth of strata / m	Stratigraphic Description	Sedimentary facies
0-11.50	Grey and dark grey clayey silt and silt, with abundant mica and white shell crumbs, interspersed with brownish clay belts in the upper part.	Alluvial flat facies
11.50-25.00	Grey, dark grey clay and clayey silt with a few silt belts, plant roots and white shell crumbs.	Flooded lake facies
25.00-27.40	Caesious silt and clayey silt with a few clay belts and a few wormholes and plant roots.	Shallow-lake facies
27.40-30.70	Yellowish grey medium-coarse sand and gravel with a few belts of greenish silt, fine sand and brownish yellow clay, with wavy bedding and a few wormholes in the upper part and numerous rust spots in the bottom.	Alluvial facies
30.70-34.44	Brownish yellow clay with a few belts of greenish grey clayey silt, more clayey silt lens and more rust spots, wind-formed loess	Continental facies (eolian loess)
34.44-37.20	Greenish, green clayey silt and silt with medium-fine sand at the bottom, gradually finer in size from the bottom to the top, with a few mica	Shallow-lake facies
37.20-60.50	Brownish yellow and yellowish grey sandy pebble gravels, mainly medium-coarse sand, pebbles and gravels; gravels poorly to well rounded, various colours, occasional brownish yellow clay belts and greenish grey and greyish purple medium-coarse sand	Alluvial facies
60.50-74.50	Brownish red, dark red siltstone, with strong weathering and soil forming processes, argillaceous-silty cementing, a lot Fe-Mn nodules and greyish-white clay belts, with a few gravels	River-lake facies
74.50-83.40	Brick-red and dark red mudstone and siltstone alternate with greyish, dark grey gypsum mudstone, medium weathering, with a few gypsum particles and Fe-Mn nodules.	River-lake facies

(Table 3). The stratigraphy in central part is characterized by a thick layer of sandy pebble gravel occurring in 60.5 to 37.2 m depth formed by alluvial, and a lime green clayey silt layer deposited in a shallow lake at the upper part (depth 37.23 to 34.44 m) (Table 3). In addition, the lithology varies markedly between 34.44 and 25 m depth in the FC borehole, with complex sedimentary environment: from the bottom to the top, brownish-yellow clay layers, brownish-yellow gravelly medium to fine sand layers, and greenish silt layers occur in sequence. In the upper part of the FC borehole (depth 25 to 0 m), clay, silty clay, and clayey silt formed in alluvial sedimentary environment alternate regularly, and the sediment in this part of the core is significantly finer-grained compared to the rest of the stratigraphy (Table 3).

OSL results

As shown in Table 1, in the seven OSL ages obtained from the ZF borehole, all samples belong to the Holocene, except for ZF-013, which belongs to the Late Pleistocene (Q_3). The stratigraphic characteristics of the stratigraphy suggest that the stratigraphy in 25 to 0 m depth belongs to the Holocene. The erosional interface at the base of the loose sand and gravel layer at 42.5m depth is taken as the lower boundary of the Holocene (Q_4) (Yu and Huang, 1996a; Yu and Peng, 2008; Su et al., 2019), which is consistent with the stratigraphic and chronological results of borehole DS08 (Figure 2). According to Yang (2008) and Su et al. (2019), combining lithological features with dating results, the depth in 47.1 to 42.5 m in sample ZF-013 is judged to belong to the late Last glacial period. In addition, because our sampling site is close to the river channel, affected by the change

of the Yangtze River and the Qingyi River channel and the strong scour of the river, some of the bottom sediments have been vertically displaced by strong hydrodynamics since the Pleistocene, caused reversal of stratigraphic, just as the age of ZF-005 and FC-003 samples (Table 1). The samples collected in 48.75 to 47.1 m depth contained a large number of pebbles and gravels, which had poor signals during testing. They could only be judged to belong to the Neogene (N) based on their lithological characteristics, with the top boundary of the formation dated to about 23.3 Ma and the bottom boundary still uncertain (Qiu, 1988; Yu and Huang, 1996b; Xu et al., 2018). Combined with the study of the lithology of the Late Cretaceous strata in the Lower Yangtze River area (Xiang et al., 2009; Xu et al., 2018), it is inferred that the bedrock at the bottom of the ZF borehole belongs to the diorite-porphyrite formed by large-scale volcanic activity in the Late Cretaceous period, and the age of the top boundary of this section corresponds roughly to 65.5 Ma, while the base cannot be determined yet.

Eight OSL ages were obtained in borehole FC (Table 1), of which the dating data for FC-001, FC-003, FC-005 and FC-006 were similar to those obtained in borehole DS08 at the corresponding levels (Figure 2), proving that this part of the formation (depth 25 to 0 m) belongs to the Holocene and using the base of the loose sand and gravel layer as the bottom boundary of the Holocene (Yan and Huang, 1991; Su et al., 2019). Based on dated data of FC-008 and FC-010 (depth 34.44 to 25 m), both are inferred to belong to the Upper Late Pleistocene (Q), while the lower part of the Upper Late Pleistocene stratigraphy is missing in the ZF borehole in conjunction with studies by Yu and Huang (1996a) and Su et al. (2019). The dated age of FC-012 obtained in 37.2 to
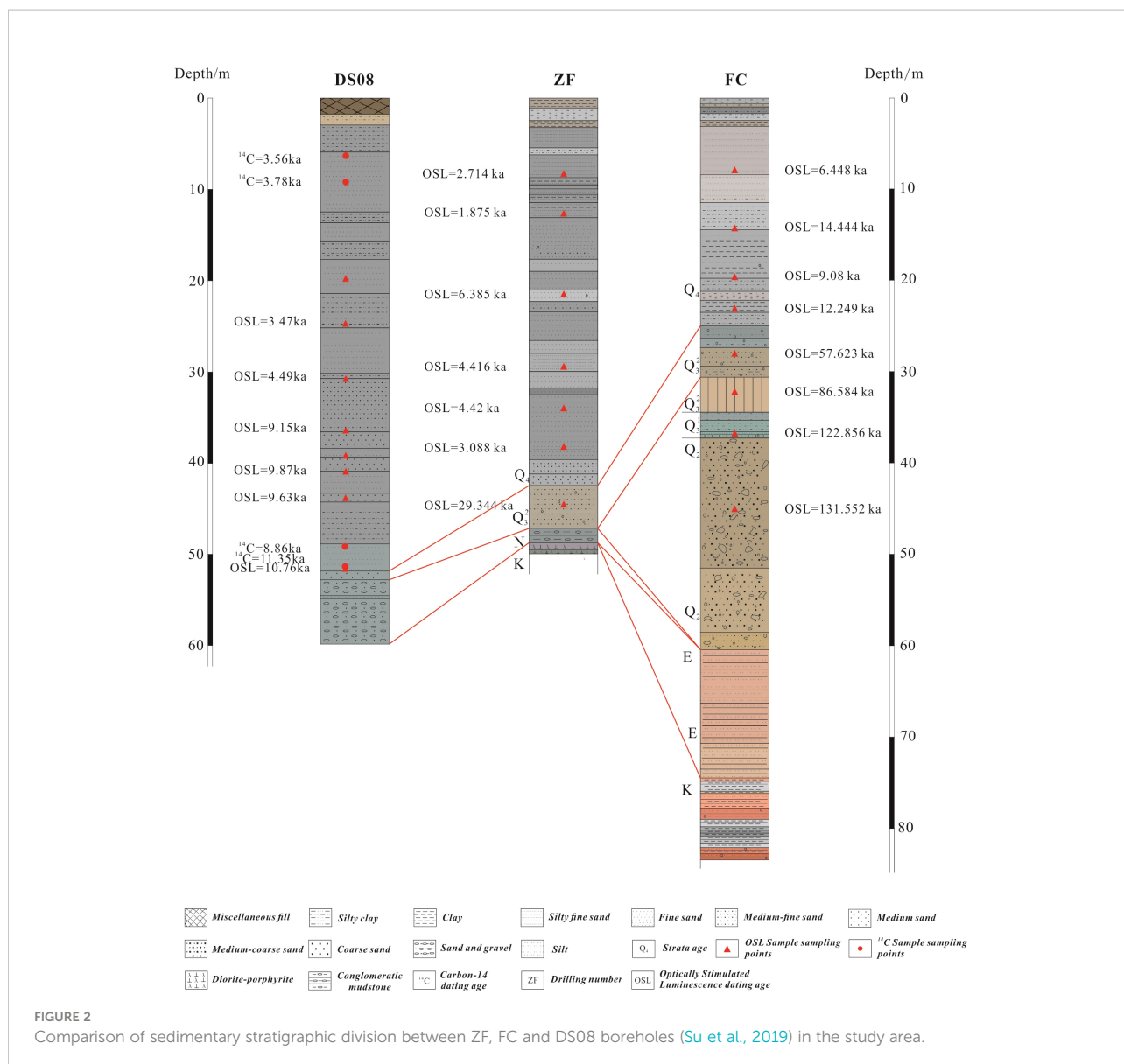
FIGURE 2

Comparison of sedimentary stratigraphic division between ZF, FC and DS08 boreholes (Su et al., 2019) in the study area.

34.44 m depth belongs to the early Late Pleistocene age (75-128 ka) (Zhang et al., 2015), and it can be inferred that the boundary between the lime green silty clay layer and the brownish yellow loess layer is the demarcation line of the Late Pleistocene lower and upper strata combined with pre-studies (Li, 1987; Yu and Peng, 2008). According to studies of lithology and age in the Middle Pleistocene stratigraphy along the lower Yangtze River, it was found that the giant thick sand and gravel layer in FC borehole in 60.5 to 37.2 m in depth belong to the Middle Pleistocene and is the top boundary (Yan and Huang, 1996a; Su et al., 2018). In addition, based on the study of the segmented lithologic characteristics of the Paleogene strata in Anhui Province, it is judged that the brick red siltstone and

mudstone in74.45 to 60.5 m depth belong to the Paleogene Period, and the top and bottom boundaries of the strata are inferred to be 33.7 and 40.3 Ma, respectively (Li, 1984; Li, 1987; Zhang et al., 2015; Xu et al., 2018). As with the strata in 74.45 to 60.5 m depth, no dating data were obtained at the FC borehole in 83.4 to 74.45 m depth. Combined with the stratigraphic lithology research of Qiu (1988); Chen (2008) and Jiang et al. (2019), the brownish to light red siltstone and grayish white to dark gray gypsum mudstone at the bottom of the FC borehole belong to the upper strata in the glutenite member of the Late Cretaceous Xuannan Formation (Chen and Xia, 1985; Li, 1987), which leads us to infer the top and bottom boundary ages are 65.5 and 70 Ma, respectively.

Grain size characteristics

The grain size composition of the core sediments from borehole ZF is dominated by sand and silt, followed by clay and gravel, with average percentages of 64.33%, 27.47%, 6.98%, and 1.11%, respectively (Figure 3; Table 4). The mean grain size (M_Z) of the sediment varies from 0.4 to 7.08φ with significant fluctuations, and the values are higher in 48.75 to 49.9 m depth and in the top stratum, mostly ranging from 2.03 to 5.9φ. Skewness (S_K) varies from -0.64 to 0.32 and is mainly symmetrically distributed between depths 49.9 to 48.75 and 47.1 to 42.5 m; whereas most of the core sediment in the ZF borehole (depth 42.5 to 0 m) has significantly lower values than the lower strata, with positive skewness and negative skewness. The sorting coefficient (S_O) of sediment grain size in the ZF borehole ranges from 1.49 to 34.47, with larger values below 42.5m depth, where sorting is very poor to poor, and above 42.5m depth, the sorting coefficient fluctuates less, up to 7.42 only, with sorting from good to moderate. The kurtosis (KG) varies between 0.59 and 2.45. From the depth of 48.75m to the top, the sediment kurtosis values are low, reaching a maximum of 2.01, mainly moderate to normal kurtosis. In 49.9 to 48.5m depth, the kurtosis values increase and vary considerably: the lower strata are mainly flat and normal kurtosis, the middle strata are narrow-normal-broad kurtosis, and the upper strata are moderate-broad kurtosis. In addition, each sample of ZF borehole sediment is mainly located in zones IV, V, VI and VII in the C-M (the graph drawn by applying the C value and M value of each sample, where C is the particle size corresponding to

the particle content of 1% on the cumulative curve of particle size analysis data, and M value is the particle size corresponding to 50% on the cumulative curve) diagram (including the low turbulence sedimentation zone without clear boundary between VI and VII), and a small amount is distributed in all other zones, which reflecting that sediments in ZF borehole are mainly transported by rivers. Among them, the sample points in zones IV and V show mainly suspension transport, but contain a small amount of rolling transport components (Figure 4).

The sediment composition of the FC borehole is dominated by silt, followed by clay, sand and gravel, with average percentages of 53.74%, 20.61%, 11.21, and 14.59%, respectively (Figure 3; Table 5). The mean grain size in FC borehole varies mainly from -3.82 to 6.73, with significant fluctuations, of which the mean grain size tends to gradual increase in 25 to 0 m depth. The sediment skewness coefficient fluctuates significantly in the range of -0.47 to 0.88, of which the skewness shows negatively and symmetrical distribution between depths 74.45 to 60.5 and 34.44 to 25 m, while the rest of the stratum shows a symmetrical and positive skewness distribution with coarse grain size. The sorting coefficients mainly belong to 0.31-5.04, with minor fluctuations and poor overall sorting in the FC borehole. In addition, the kurtosis is concentrated chiefly between 0.54 and 2.96 with slight fluctuations in which the kurtosis is mostly very narrow in the stratum below 60.5m depth and moderate or constant in 60.5 to 37.2m depth. And between 37.2 and 34.44m depth, the kurtosis decreases with a range of 0.84 to 1.09 which is

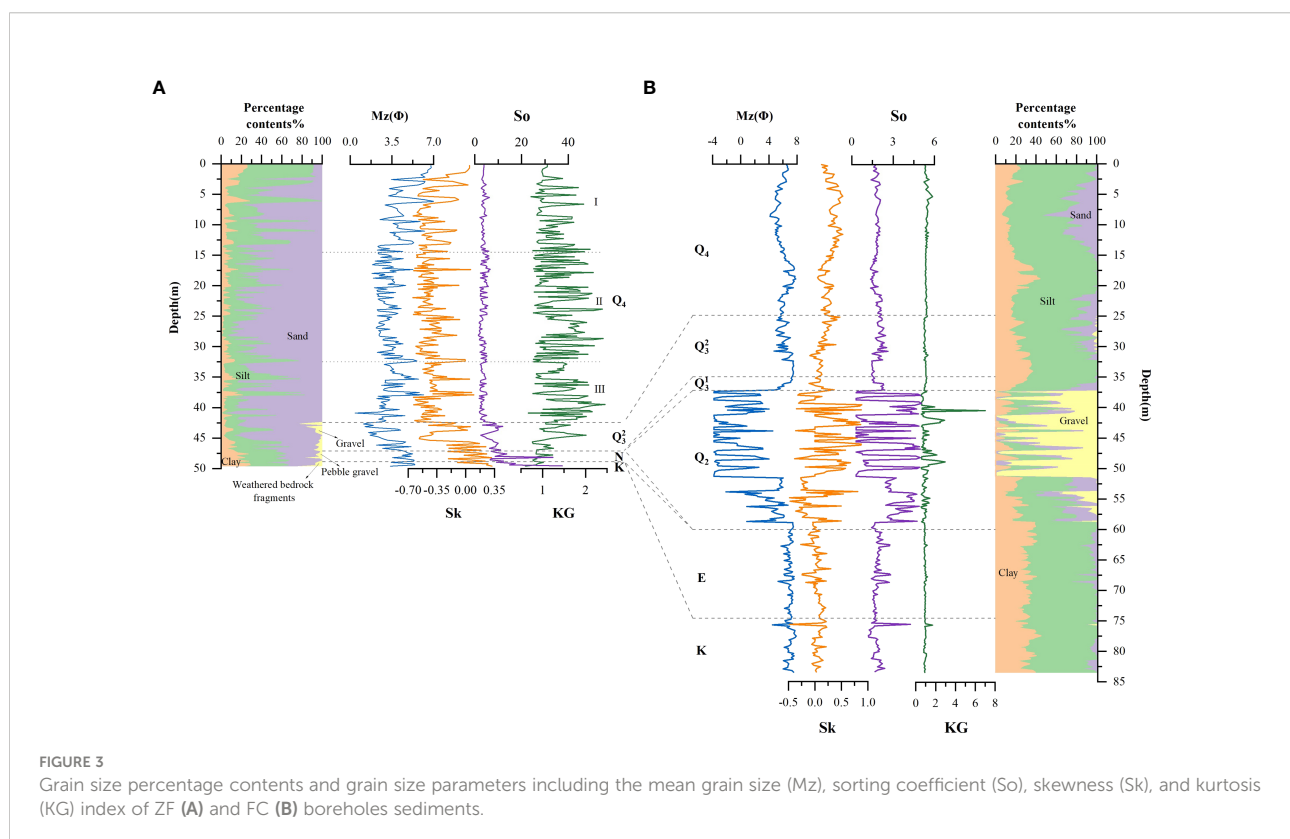
FIGURE 3
Grain size percentage contents and grain size parameters including the mean grain size (Mz), sorting coefficient (So), skewness (Sk), and kurtosis (KG) index of ZF **(A)** and FC **(B)** boreholes sediments.

TABLE 4 The grain size composition and parameters characteristics and magnetic susceptibility results of the ZF borehole in Wuhu.

	Clay (<2 μm)	Silt (2-63 μm)	Sand (2000>63 μm)	Gravel (>2000 μm)	Mean grain size (M_Z/φ)	Sorting coefficient (S_O)	Skewness (S_K)	Kurtosis (KG)	Low-frequency susceptibiliy (χ_{lf})	High-frequency susceptibiliy (χ_{hf})
Maximum	29.01%	75.93%	100.00%	28.37%	7.08	37.48	0.32	2.45	132.38	133.5
Minimum	0.00%	0.00%	0.55%	0.00%	0.41	1.50	-0.64	0.60	5.25	4.00
Mean value	6.98%	27.47%	64.33%	1.11%	3.56	4.58	-0.36	1.32	60.36	59.98
Standard deviation	6.21	16.89	22.77	3.83	1.20	3.79	0.22	0.46	25.29	25.57
Variation coefficient	0.89%	0.62%	0.35%	3.47%	0.34%	0.83%	-0.63%	0.35%	0.42%	0.43%

mainly narrow, while in the upper strata (depth 34.44 to 0 m) the kurtosis is mostly very narrow-medium. As can be seen from Figure 4, the samples of FC borehole are mainly located in zones VI, VII and VIII (including the low turbulence deposition zone without clear boundary between VI and VII) in the C-M diagram with a small number of them are distributed in other zones, which represents complex sedimentary dynamic conditions. Among them, the sample points in zones IV and V show mainly suspension transport, but contain a small amount of rolling transport components.

Magnetic susceptibility and chromaticity characteristics

Both high and low-frequency magnetization values of the ZF borehole sediments were high and fluctuating, with mean values of 64.3×10^{-8} m³/kg and 64.67×10^{-8} m³/kg for high and low-frequency magnetization, respectively. And the chromaticity (L*, a*, and b*) varied significantly, of which a lesser extent fluctuating of L*(Figure 5; Table 4). The magnetization rate gradually increased with the depth in 49.9-48.75 m, with no significant changes in brightness (L*) and redness (a*), while yellowness (b*) showed a trend of first decreasing and then increasing. The magnetization values in 48.75 to 47.1 m depth significantly increase with depth and a small range of chromaticity fluctuations. In 47.1 to 42.5 m depth, the magnetization values are minor and do not fluctuate wildly, with a trend of increasing and then decreasing with depth and a higher peak value, while a* and b* show significant sub-level changes, and b* shows a considerable increase. The magnetic susceptibility and chroma of sediments in 42.5 to 0 m depth changes frequently and violently, while the magnetic susceptibility showed a stable-increase-decrease trend with the rise in depth and the chroma showed a regional stability after violent fluctuations, of which the maximum value of b* appears
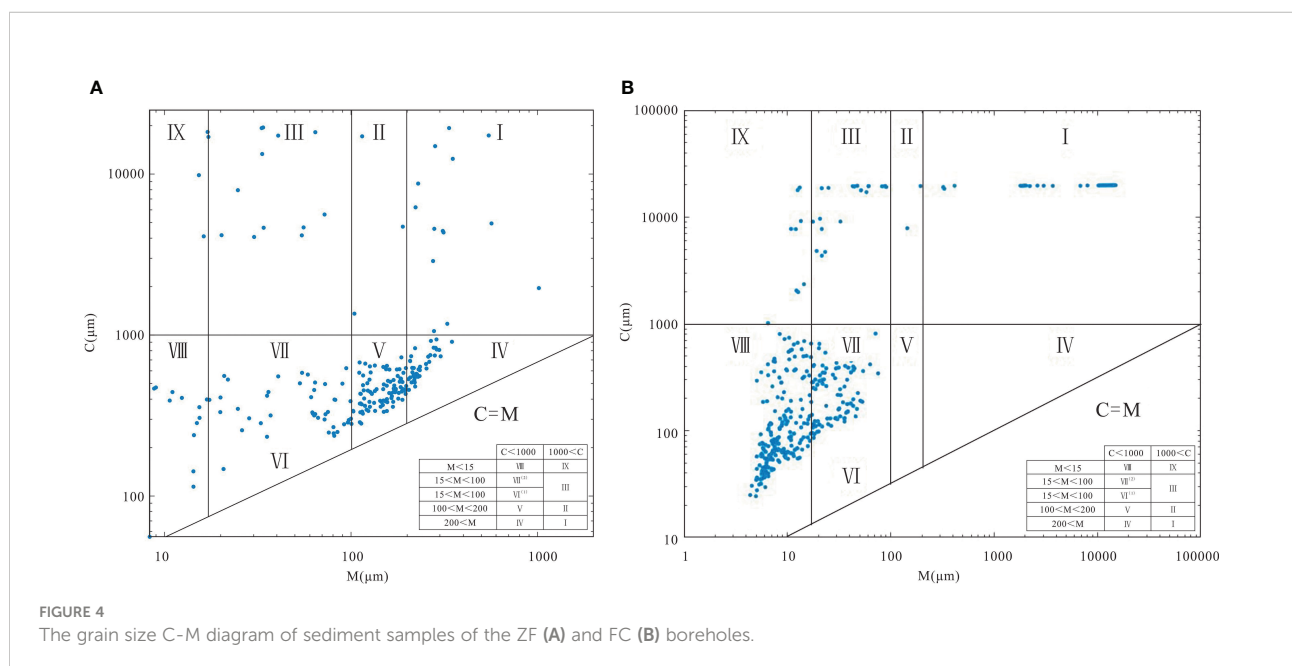

FIGURE 4
The grain size C-M diagram of sediment samples of the ZF (A) and FC (B) boreholes.

TABLE 5 The grain size composition and parameters characteristics and magnetic susceptibility results of the FC borehole in Wuhu.

	Clay (<2 μm)	Silt (2-63 μm)	Sand (2000>63 μm)	Gravel (>2000 μm)	Mean grain size (M_Z/φ)	Sorting coefficient (S_O)	Skewness (S_K)	Kurtosis (KG)	Low-frequency susceptibiliy (χ_{lf})	High-fre-quency susceptibiliy (χ_{hf})
Maximum	44.77%	86.56%	56.54%	100.00%	7.91	5.04	0.88	7.01	66.25	66.63
Minimum	0.00%	0.00%	0.00%	0.00%	-3.82	0.31	-0.48	0.54	0.88	0.63
Mean value	20.61%	53.74%	11.21%	14.59%	4.91	2.06	0.14	1.01	9.50	9.51
Standard deviation	11.31	23.01	12.27	30.96	3.37	1.01	0.24	0.42	8.86	8.84
Variation coefficient	0.55%	0.43%	1.09%	2.12%	0.69%	0.49%	1.67%	0.42%	0.93%	0.93%

in the lower part accompanied by L* is negatively correlated with a*.

The magnetic susceptibility values of the FC borehole deposits are low, the fluctuation range is extensive, and their chromaticity varies significantly with depth (Figure 5; Table 5). In 83.4 to 74.45 m depth, the magnetic susceptibility has multiple abnormal peaks, and the overall trend is gradually increasing with the increase of depth, in which the variation range of L* is small and both a* and b* show a trend of first decreasing and then increasing. The change of magnetic susceptibility in the depth of 74.45 to 60.5 m is insignificant, in which the average values of low-frequency and high-frequency magnetic susceptibility are 6.98×10^{-8} m³/kg and 6.95×10^{-8} m³/kg, respectively. In addition, except an immense valley value at 72.9 m of the brightness (L*), the change of chromaticity is slight, which indicating that the redox environment is relatively stable. The overall value of magnetic susceptibility in 60.5 to 37.2 m depth is relatively low, of which the variation range of high and low-frequency magnetic susceptibility is 0.625 to 54.625×10^{-8} m³/kg and 0.875 to 53.5×10^{-8} m³/kg. In contrast, the chromaticity fluctuates violently, of which L* and a* was negatively correlated while b* showed a significant increase. In 37.2 to 34.44 m depth, except a peak appears at 35.41 m, the change range of magnetic susceptibility is relatively stable with the low value, and the ranges of high and low-frequency magnetic susceptibility are $2.25-9.875 \times 10^{-8}$ m³/kg and 2.375 to 11.75×10^{-8} m³/kg, in which in 34.44 to 25.0 m depth the magnetic susceptibility decreases significantly. However, the variation of L* of is relatively gentle and still has a negative
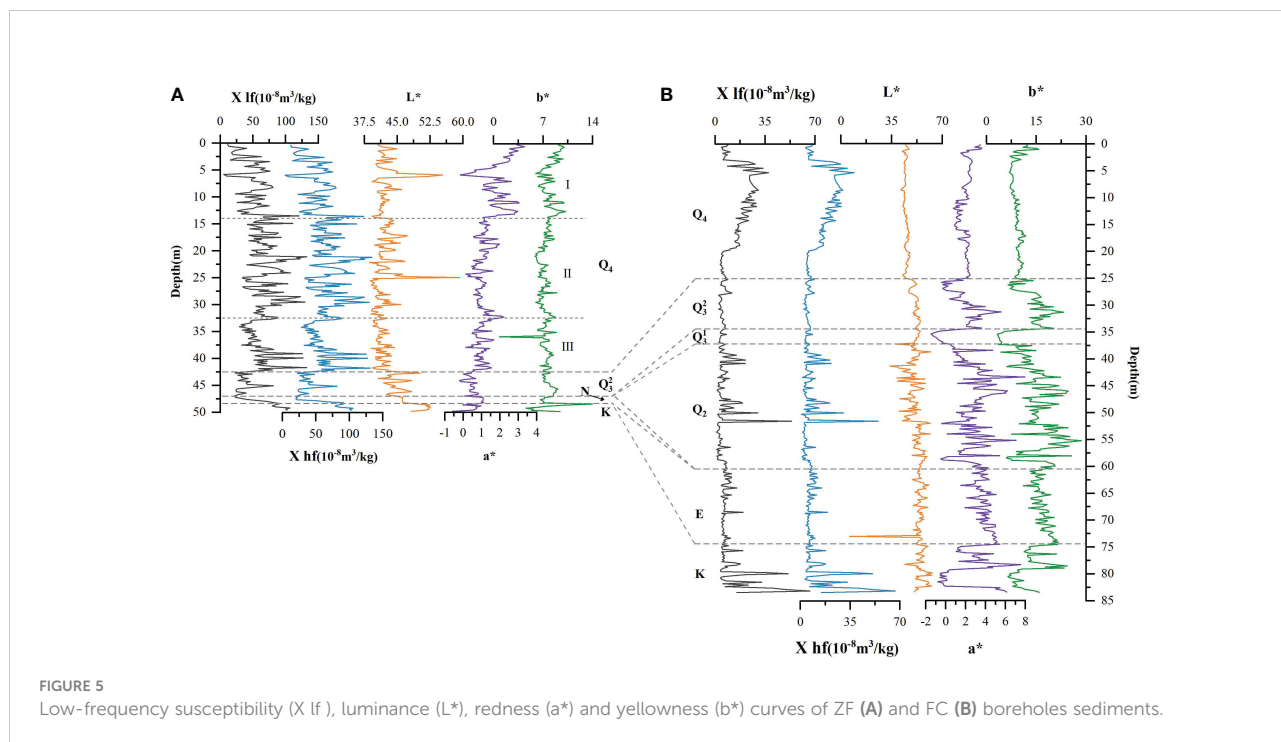

FIGURE 5
Low-frequency susceptibility (X lf), luminance (L*), redness (a*) and yellowness (b*) curves of ZF **(A)** and FC **(B)** boreholes sediments.

correlation with a*. In the upper strata of the FC borehole (depth 25.0 to 0 m), the magnetic susceptibility fluctuates wildly, in which a peak at about 5.3 m occurs while a relatively significant decrease until approximately 19.67 m shows with a minimum value. And the fluctuation range of chromaticity in the 25.0 to 0 m depth is relatively stable, of which the variation ranges are 41.20 to 47.69 (L*), 0.74 to 3.63 (a*), and 6.86 to 15.78 (b*), respectively.

Discussion

Sedimentary environment evolution

The sedimentary history of eastern China is closely related to climate, sea-level changes and regional tectonic activity (Wei, 2003; Chen et al., 2009; Zhang, 2016; Cui, 2017; Landwehrs et al., 2021). In particular, the collisional subduction of the North China Plate with the Yangtze Plate and the interaction of the paleo-Pacific plate with the Eurasian Plate have had a profound impact on the marine and terrestrial sedimentation of eastern China (Li, 1987; Han, 2016).The sedimentary records from the ZF and FC boreholes and their chronostratigraphic framework features demonstrate that fluvial and lacustrine deposits have dominated the study area since the Late Cretaceous (Li, 1987; Qiu, 1988; Cao et al., 2006). Different deposits developed along the two banks of the river, and the western bank was intruded by magma to form amphibolites during the Late Yanshanian (Zhang and Huang, 1989; Yu and Xu, 2009). Afterwards, the area was absent from deposition for a long time or was consumed by intense weathering and denudation (Bai et al., 2007). However, there are alternating gypsiferous mudstones and siltstones in the Late Cretaceous east coast in a fluvial-lacustrine stage. The poor overall grain size sorting of sediments in this profile (Figure 3) indicates that the east coast was significantly influenced by watershed variability and unstable hydrodynamic environments, consistent with the low-energy depositional environments of lakes, alluvial fans, and fluvial floodplains (Cao et al., 2006; Chen, 2020). By the early Tertiary Eocene, thicker layers of brick-red siltstone with more gypsum and ferromanganese nodules and carbonaceous mudstone bands were deposited on the east bank of the Yangtze under hot and dry climatic conditions (Chen and Xia, 1981; Zhu, 2020), but not on the west bank of the Yangtze. The variation of magnetization and colorimetric indicators in the FC borehole sediments (Figure 4) indicates that the hydrodynamic conditions were weak during the Early Tertiary-Cenozoic period and the redox environment along the east bank of the river was more stable. Compared with the Early Tertiary-Cenozoic, the Late Tertiary is characterized by under-deposition on the east bank and the development of pebbles and conglomeratic mudstones on the west bank in a high-energy alluvial fan depositional environment (Chen and Xia, 1981; Qiu, 1988). In addition, the frequent uplift of the late Himalayan crust stripped away the

thick alluvium that had formed in the region, resulting in a general absence of early Pleistocene sediments in the study area (Xu et al., 1987; Fang, 2005; Pu et al., 2012). Similarly, under the differential sedimentation activity since the Cenozoic, there is no middle to late Pleistocene sedimentary stratigraphy on the west bank of the Yangtze River (Qiu, 1988). In the context of frequent alternation of dry and hot and humid climates in the Middle Pleistocene, the riverbeds on the east bank of the Yangtze have considerable specific fall characteristics, forming a typical fluvial alluvial depositional environment (Xu et al., 1987; Qiu, 1988).In the Middle Pleistocene, against the background of drastic changes in climatic and hydrological conditions, the riverbed on the east bank of the river had a considerable specific drop, forming a typical fluvial alluvial depositional environment (Xu et al., 1987; Qiu, 1988). In the high-energy fluvial alluvial environment, combined with geo-environmental factors such as mechanical and chemical weathering formed on both sides of the upper reaches of the river, as well as the extensive distribution of large amounts of loose clastic material transported by mountain glaciers, the sedimentary depressions on the east bank gradually received deposition during generation and rapidly accumulated a massively thick layer of muddy gravel (Qiu, 1988; Hu et al., 2016). By the late Middle Pleistocene, the crust had stabilized and the sinkholes were filled in mainly by receiving interactive deposits of sand and gravelly clay layers. Lime green and green clayey silt dominated the study area in the early Late Pleistocene and the river hydrodynamic conditions weakened (Yan and Huang, 1999; Gu, 2005; Fan et al., 2006; Luo et al., 2015). Subsequently, the cold and dry climate of the Last Glacial Period deposited a group of loess-like clay layers on the east bank of the Yangtze River, known as the Xiashu Formation (Yu and Huang, 1996b; Shao, 1999). These homogeneous and massive loess-like clays may be the product of massive flooding that began at the end of the Dali Ice Age (Yu and Huang, 1996b; Shao, 1999; Song, 2014). After the recession of solid river erosion, subsequent deposition was relatively weak, with only moderately thick green to yellowish gray medium to fine sandy alluvium deposited in the upper part of the Lower Shu Loess (Yan and Huang, 1991; Li, 2014).

In general, the west bank of the Yangtze River is constrained by the geomorphic pattern, and climate change has less influence on deposition, while hydrodynamic conditions have more influence on the area (Su et al., 2019). In the late Late Pleistocene, borehole DS08 (Figure 2) deposited only a thin layer of green fine sand, which is similar to the Middle-Late Pleistocene upper stratigraphy on the east bank of the Yangtze River, demonstrating the complexity of the depositional environment and the difference in geomorphology between the east and west banks of the Yangtze River during the Late Pleistocene (Qiu, 1988; Su et al., 2019).In the early Holocene the study area was at a low sea level formed at the apex of the Tali glaciation, and fluvial erosion dominated by downcutting was prominent in the valley (Li, 1987; Qiu, 1988; Wei, 2003; Su et al.,

2019). By the middle of the Holocene, sand layers of different grain thickness were deposited along the west bank of the Yangtze under the influence of the Yangtze main current, creating a depositional environment of river alluvium. Meanwhile, the east bank of the Yangtze River was in a low-energy and more closed hydrodynamic environment under the influence of the lower Qingyi River basin, and riverine muddy clays were commonly deposited (Figure 2).

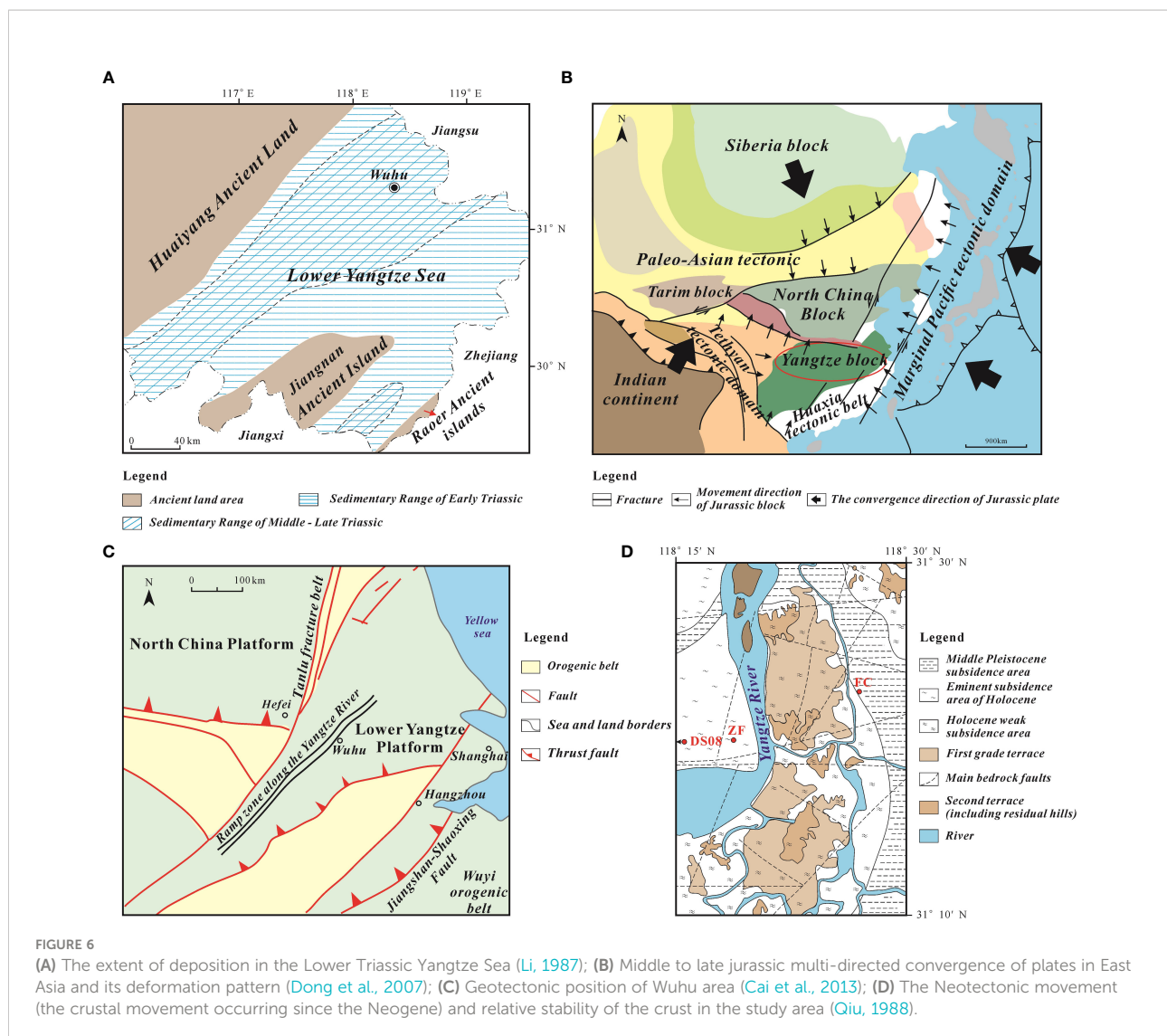## Sedimentary process influenced by crustal movement

Since the Mesozoic, eastern China has undergone a long and complex tectonic evolution, with major orogenic belts undergoing resurgence and revival, magmatism and extensional movements (Zheng et al., 2013; Xu et al., 2021; Wang et al., 2022). The paleomorphology of the sedimentary basins in the study area is constrained by the tectonic evolution of the riverine basin complex in the lower Yangtze River, which consequently affected the evolution of rivers, their hydrodynamic conditions, and their sedimentary characteristics (Wei, 2003; Xu et al., 2018).

During the Mesozoic, the Indo-China movement in the Middle and Late Triassic completely withdrew seawater from the study area, and terrestrial sedimentation developed from the subduction (Figure 6A). Under the collision and subduction of the Pacific and Eurasian plates (Figure 6B), the area experienced large-scale magmatic intrusion and tectonic deformation during the Middle and Late Jurassic. From the Jurassic to the Cretaceous, the Izanagi Plate began to subduct to the Eurasian plate, and the Yanshan movement led to unprecedented exuberant magmatism and orogeny in eastern China (Hou, 2005; Zheng et al., 2013; Yang et al., 2016; Qiu et al., 2018).

From Late Jurassic to Cretaceous, the Izanagi Plate began to retreat after low angle subduction, and the Yanshan movement led to unprecedented magmatism and orogeny in eastern China (Hou, 2005; Zheng et al., 2013; Tan et al., 2020; Wu et al., 2020). The riverine region was a tectonically tense environment with well-developed terrestrial volcano-sedimentary basins and an overall development of coal-bearing clastic deposits in the Early to Middle Jurassic inland lake and river stage (Qiu, 1988; Hou, 2005; Wang et al., 2012; Zhong, 2010; Li, 2020). During the Late Jurassic period, the lower Yangtze River region entered a synclinal phase under the control of the Yanshan movement, and large-scale block movements and magmatism occurred in the region, reaching a peak in the Early Cretaceous (Qiu, 1988; Hou, 2005; Zheng et al., 2013; Wu et al., 2020). At the same time, uneven ground uplift dominated the region, and a series of north-east-trending volcano-sedimentary fault basins and pull-apart basins developed, forming a basin-ridge tectonic pattern (Qiu, 1988; Dong et al., 2007; Zhang et al., 2014). The western bank of the Yangtze River in the study area received moderately

acidic magmatic intrusion during the first phase of the Late Yanshan period and lacks Paleoproterozoic (E) sedimentary stratigraphy (Sun and Peng, 1987; Qiu, 1988). Moreover, its maximum depth is only 48.85 m, which is consistent with the intense surface uplift activity that began in eastern China during the mid to late Cretaceous (Hou, 2005; Qu, 2011). In the late Late Cretaceous, magmatic activity weakened and basically stopped, and the east bank of the river was in a relatively stable period of tectonic subsidence, with a large overall subsidence. The topographic uplift was large, forming the North Steep Gate Depression, which received continuous deposition of lacustrine and alluvial fan-phase red conglomerate composite terrestrial clastic tectonics and Paleozoic river-lake conglomerate silt (Qiu, 1988; Xu et al., 2018). Under the Yanshan and early Himalayan movements, the fault block movement in the study area was active for a long time, forming NE-NNE, near-EW and NW-trending faults (Figure 6D), leading to differences in depressional basin development and sedimentary stratigraphy in the area.

Since the Cenozoic, eastern China has inherited the Mesozoic fault-basin tectonic pattern. In the background of continuous subduction of the Pacific plate and successive collisions of the Indian and Eurasian plates, the study area was uplifted overall but subducted locally, dominated by Neotectonic differential uplift movements (Qiu, 1988; Yang and Li, 1998; Li, 2017; Xu et al., 2018; Zhu et al., 2020; Wang et al., 2021). In addition, early Neotectonic activity was dominated by inheritance, while later differential expression was more prominent and unstable movements continued throughout the Neotectonic period (Chu et al., 2008; Song et al., 2008). During the Late Oligocene, a unified fault basin system was formed along the Yangtze River in the lower Yangtze River region (Figure 6C). In contrast, during the Cenozoic, tectonic uplift movements in the lower Yangtze River region were characterized by strong east-west and weak central parts, and extensively uplifted sedimentary rocks were exposed to weathering and denudation (Li, 1987; Chu et al., 2008; Xu et al., 2018). Under the influence of differential uplift movements, the east bank of the Wuhu riverine area has been in the uplift erosion-exfoliation zone and lacks sediments from this period (Sun and Peng, 1987; Xu, 2008). Han's study proposed that the absence of Early Pleistocene fluvial deposits along the river in this area is due to the long-term relative stability and slight subsidence of the crust during the Early Pleistocene. However, at the end of the Early Pleistocene or the beginning of the Middle Pleistocene, the crust experienced extensive and distinct unequal upward movements (Qiu, 1988; Li, 2017; Xu et al., 1999). Tectonic movements at the end of the Middle Pleistocene caused significant uplift in the region, with extensive erosion on the west bank of the river in the region and increased subsidence on the east bank, increasing the slope of the river channel and receiving deposits of giant thick gravel layers, which then gradually stabilized (Xu et al., 1999; Chu et al., 2008; Guo, 2020). Thicker Middle Pleistocene sediments occur only in the

FIGURE 6
(A) The extent of deposition in the Lower Triassic Yangtze Sea (Li, 1987); **(B)** Middle to late jurassic multi-directed convergence of plates in East Asia and its deformation pattern (Dong et al., 2007); **(C)** Geotectonic position of Wuhu area (Cai et al., 2013); **(D)** The Neotectonic movement (the crustal movement occurring since the Neogene) and relative stability of the crust in the study area (Qiu, 1988).

study area and in a narrow zone between Tanggou and the mouth of Yuxi, indicating a clear zone of inherited sedimentation within this range (Figure 6D). During the early to middle Late Pleistocene, only thin clayey chalk and chalk layers were deposited along the east bank of the river in this area, indicating another strong development of Neotectonic movement (Li, 2017; Chu et al., 2008). However, the development of upper Late Pleistocene deposits of modest thickness along the river banks at the end of the Late Pleistocene does not demonstrate that Neotectonic movement was still strongly active during this period, as the distribution of the lower Holocene gravel layer is stable and comprehensive. All the strata below the sand layer were strongly eroded, while there is a clear erosional interval. The above features indicate that the sediments in the upper part of the Late Pleistocene were destroyed and reduced in thickness by the intense scouring and erosion of the Holocene rivers (Yan and Huang, 1999),

which further verifies that the strong differential uplift movement in the Middle Pleistocene has ended and the tectonic setting of the region has turned relatively stable (Qiu, 1988; Li, 2017). As shown in Figure 2 and Figure 6D, although the Neotectonic movement in the study area is complex, the dominance of subsidence activity is obvious, and there are significant differences in Holocene Neotectonic subsidence movements bounded by the two banks of the Yangtze River (Qiu, 1988; Xu et al., 1999). The west bank of the river receives thicker fluvial alluvium and fluvial deposits, while the east bank is dominated by lacustrine deposits followed by fluvial alluvial phases. The demarcation line between the weak and significant sedimentation zones is presumed to be roughly at the present-day location of the Yangtze River, due to the fact that the present-day riverbed location is essentially the most recent location of the Yangtze River, as the Yangtze River has continuously moved southeastward throughout its history, and

neotectonic movements have constrained the general trend of riverbed migration in the Yangtze River (Qiu, 1988; Jin et al., 2015; Zhang et al., 2018b). The above features suggest that Neotectonic movement increased regional differences during the Holocene period and shaped the present-day geographic pattern.

Response of sedimentary environment to climate and sea-level change

To explore the response of terrestrial sedimentary systems to environmental change since the Late Cretaceous at a regional scale, terrestrial sedimentary records from regional boreholes were compared with known climate-sea level change records. The Late Cretaceous, the Neogene, and the Middle Pleistocene to Holocene deep-sea oxygen isotope stages of the sedimentary record in the study area were dated to 65.5-70 Ma, 33.8-40.4 Ma, 147.54 -128 ka BP (MIS 6), 128-117 ka BP (MIS 5), 117-58 ka BP (MIS 4), 58-25 ka BP (MIS 3), 25-11.55 ka BP (MIS 2), and 11.55-4.65 ka BP (MIS 1), respectively (Figures 7–9).

The Cretaceous was a period of greenhouse climate with higher atmospheric CO_2 concentrations and sea levels than today (Nordt et al., 2003; Davies et al., 2009; O'Brien et al., 2017; Tierney et al., 2020). The widespread construction of red gravelly complex

terrestrial debris deposits in eastern China suggests that this period was still a period of high temperatures, as the extensive climatic and marine records indicate (Xu, 2008; Wang et al., 2014; Zhang et al., 2018a) that greenhouse climate changed and evolved rapidly during the Late Cretaceous (65.5-70 Ma) (Bornemann et al., 2008; Xiang et al., 2009; Wang et al., 2021; Yan et al., 2022), and greenhouse climate change and rapid evolutionary turnover during the Late Cretaceous (65.5-70 Ma). The Pacific Ocean (Cloetingh and Haq, 2015), global sea level change (Miller et al., 2005), and SST (Jiang et al., 2021a) records indicate extensive sea erosion, significant oceanic climate, and frequent sea surface fluctuations during this period (Figure 7). The mean grain size, redness, and low-frequency magnetization of the sediments follow a similar trend during this period (Figure 7). Around 70-69.3 Ma, higher values of magnetization and redness and smaller mean grain size of the core sediments are consistent with global warming, gradual sea level rise in the northwest Pacific Ocean, and decreasing $\delta^{18}O$ values recorded at Dongge Cave, China, during this period (Figure 7). During the period 69.3-67.2 Ma, with higher but decreasing temperatures in eastern China, gradual global sea level rise, and the influence of river oscillations in the region, mudstones generally developed in more arid conditions in a lower energy environment in a confined environment, with the period and increasing water depths can be found in sediments with significantly lower redness and magnetization than before (Zhang, 2016; Huang and Han, 2019).
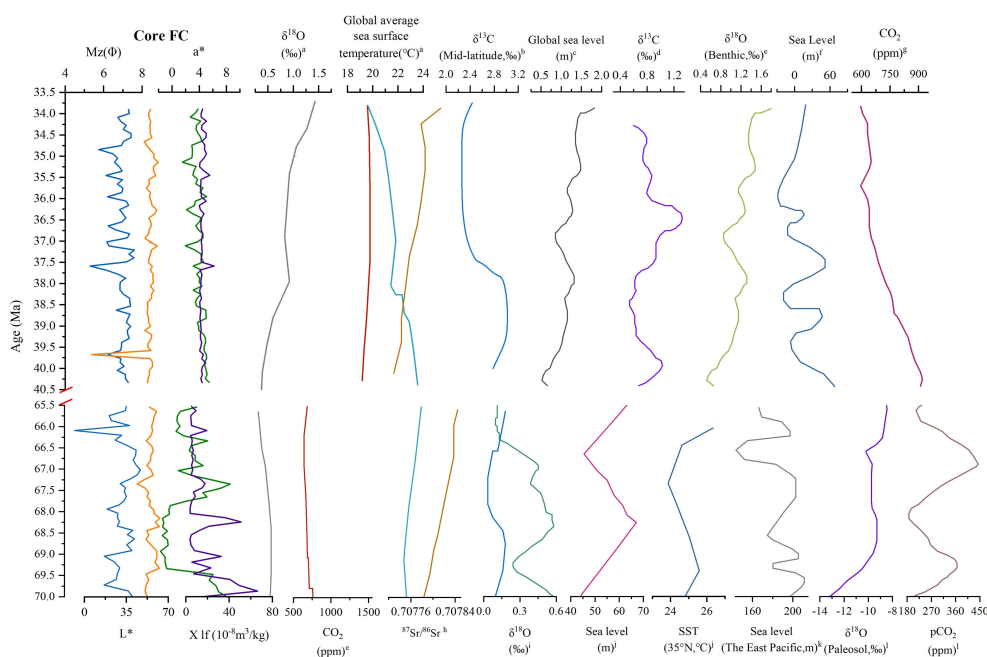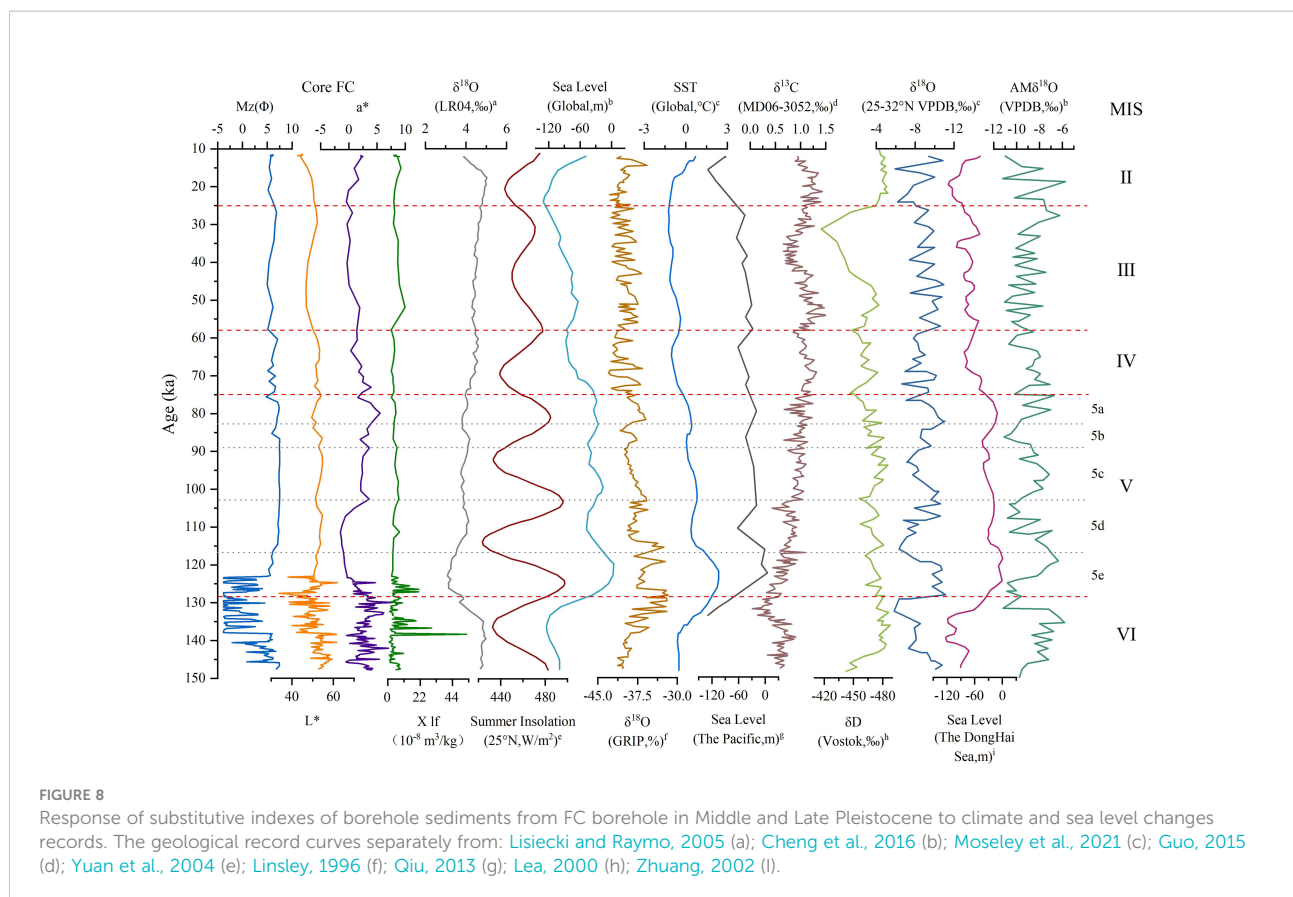

FIGURE 7
Response of substitutive indexes of borehole sediments from FC borehole in Neogene and Late Cretaceous to climate and sea level changes records. The geological record curves separately from: Mills et al., 2019 (a);Prokoph et al., 2008 (b); Lin and Sun, 1985 (c); Westerhold et al., 2020 (d); Foster et al., 2017 (e); Wu et al., 1998 (f); Hansen et al., 2013 (g); McArthur et al., 2012 (h); Barrera and Savin, 1999; Friedrich et al., 2012 (i); Jiang et al., 2021 (i); Cloetingh and Haq, 2015 (k); Gao, 2015 (l).
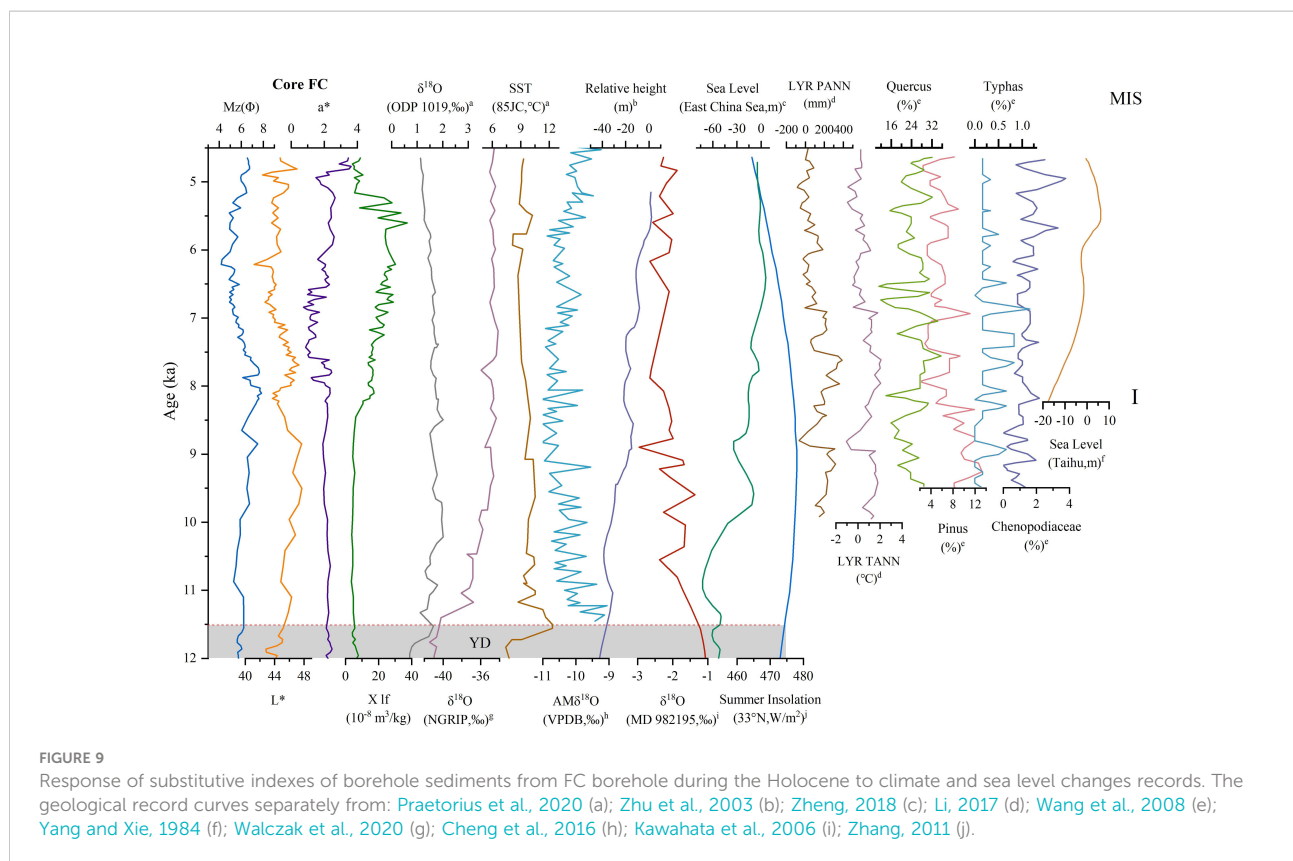
FIGURE 8

Response of substitutive indexes of borehole sediments from FC borehole in Middle and Late Pleistocene to climate and sea level changes records. The geological record curves separately from: Lisiecki and Raymo, 2005 (a); Cheng et al., 2016 (b); Moseley et al., 2021 (c); Guo, 2015 (d); Yuan et al., 2004 (e); Linsley, 1996 (f); Qiu, 2013 (g); Lea, 2000 (h); Zhuang, 2002 (I).

During the early Neogene (33.8-40.4 Ma), corresponding to high values of global mean sea surface temperature and atmospheric CO_2 concentration (Figure 7), strongly oxidized red mudstone and the high-temperature indicator mineral calcium mannite occur in the depressional basins of the study area under the influence of early Himalayan movements (Li, 1984; Li, 1987; Zhang et al., 2015). Zhang, (2016) showed a warm, slightly humid subtropical climate with low temperatures during the Neogene and a predominance of angiosperm pollen in the study area (Zhang et al., 1986; Zhao, 1992; Jiang et al., 2012; Zhu, 2020). The combination of marine oxygen isotope, carbon isotope, and Sr isotope ratios shows that the sea level fluctuated dramatically and rose and fell rapidly and that a high-energy alluvial fan-phase depositional environment developed in the area under the effect of frequent changes in the river erosion datum (Figure 7).

During the Quaternary period, the global ice age frequently alternated with interglacial periods, and the climate was cool and dry (Gao, 2015; Jiang et al., 2021b). During the MIS 6 period (147.54-128 ka BP), the deep-sea $\delta^{18}O$ and solar radiation energy records indicate (Figure 8) that global temperatures and sea level heights were low, with an overall trend of slow decline, until around 133 ka BP, when temperatures began to rise significantly (Lisiecki and Stern, 2016; Moseley et al., 2021), and in the western Pacific and Japan Sea regions, sea level rose rapidly (Zheng et al., 2013; Qiu,

2013). At this time, the rapid accumulation of giant thick sand and gravel layers in the study area and the significantly reduced values of L^* and M_Z in the sediments suggest that the regional sedimentary record is well correlated to global climate and sea level fluctuations.

During MIS 5 (128-117 ka BP), the global climate entered an environment of frequent warm-wet-cold-dry climate alternations, in which MIS 5a, 5c, and 5e were characterized by relatively high temperatures and widespread sea erosion along the eastern coast of China (Zhuang, 2002; Grant et al., 2014; Yuan et al., 2004; Zheng et al., 2013; Moseley et al., 2021). Especially into the last interglacial (MIS 5e), temperatures and sea level heights were at high levels throughout the Pleistocene, and river hydrodynamic conditions were strong in the study area. In contrast, during MIS 5b and 5d, temperatures dropped dramatically, the climate was cold and dry, and a large drop in sea level occurred (Figure 8). Combined with deep-sea $\delta^{13}C$, ice core $\delta^{18}O$, and solar radiation records (Guo, 2015; Cheng et al., 2016; Qiu, 2013), the study found that the overall environmental change was dramatic during MIS 5, but there was still a slow decline in temperature and sea level. However, environmental proxies for sediments in the region do not show frequent drastic changes during the MIS 5 period, and only the value of a* is consistent with the global and regional climate-sea level records (Figure 8). In conjunction with Zhao, (2017) and Cheng et al. (2021), it can be found that the East Asian summer

FIGURE 9
Response of substitutive indexes of borehole sediments from FC borehole during the Holocene to climate and sea level changes records. The geological record curves separately from: Praetorius et al., 2020 (a); Zhu et al., 2003 (b); Zheng, 2018 (c); Li, 2017 (d); Wang et al., 2008 (e); Yang and Xie, 1984 (f); Walczak et al., 2020 (g); Cheng et al., 2016 (h); Kawahata et al., 2006 (i); Zhang, 2011 (j).

winds provided more precipitation to the eastern coastal region and the Sea of Japan region in the presence of dramatic global climate fluctuations.

MIS 4 was a cold phase of the early Last Ice Age, with low solar radiation energy (Cheng et al., 2016), increased global ice volume, and a relatively large sea level decline process (Figure 8). According to the sedimentary tectonic record, the regional hydrodynamic environment was not stable, and the overall L* and a* records are roughly the same as the mid-latitude stalagmite $\delta^{18}O$ (Moseley et al., 2021) and seawater PH variation (Guo, 2015) records, suggesting that the study area did not experience significant effects on the sedimentary environment due to weakened tectonic activity in a globally cold and dry climatic context and that regional wind and dust loess The accumulation of regional wind-dusted loess began (Xu et al., 2021).

At MIS 3 (25-58 ka BP), there are also significant fluctuations in temperature and sea level (Figures 8). The climate was warm and humid at the beginning of MIS 3 (Yuan et al., 2004) until around 50 ka BP when temperatures began to decline, sediment grain size gradually became more delicate, the hydrodynamic environment was less energetic, L* values increased, a* values decreased, and magnetization values decreased. According to several climatic indicators, the monsoon activity in eastern China gradually weakened during the period 25-40 ka BP, with decreasing precipitation and temperature (Yuan et al., 2004; Cheng et al.,

2016). Around 27 ka BP, temperatures gradually warmed, and sea levels rose rapidly, enhancing sedimentary hydrodynamic conditions in the study area (Figure 8).

During MIS 2 (11.55-25 ka BP), global sea level, sea surface temperature, and solar radiation decreased significantly, making it the coldest climate and most considerable glacial period of the Last Ice Age (Zhang, 2013; Cheng et al., 2016). Sediment Mz and L* values decreased during this phase, while a* tended to increase, indicating that the regional depositional environment was significantly turbulent (Figure 8). Combined with studies of stalagmite $\delta^{18}O$ at 25-32°N, sea-level changes in the East China Sea, and records of solar radiation energy at 25°N (Zhuang, 2002; Yuan et al., 2004), it was found that the study area was influenced by temperate-subtropical monsoon climate and tectonic movements in the Northern Hemisphere, with a marked increase in temperature and gradually stronger hydrodynamic conditions in rivers The study area is influenced by the temperate-subtropical climate and tectonic movements in the northern hemisphere.

During the MIS 1 phase, the Yangtze and Qingyi rivers were deposited in an agglomerated manner, developing riverine and floodplain phase sediments, which is consistent with the climate shift to a warm and humid character during this period in northern latitudes. Frequent climatic fluctuations began to occur from around 8.2 ka BP, with a slow overall rise

in sea level (Figure 9). The increase in Mz and L* during the period 8.2-11.55 ka BP with the SST and PJJA records (Ding et al., 2020) suggests that the regional sedimentary record during this period is less sensitive to the effects of global climate change, but can still reflect solid climatic fluctuations. The early part of MIS 1 (8.75-11.55 ka BP) has a warmer and wetter climate and can be identified as a period of marginal beach deposition and floodplain accretion. In contrast, the clayey and sandy interbed were formed in the late MIS 1 (4.62-8.75 ka BP), and between 8.2 and 6.3 ka BP, the region deposited sandy and clayey interbeds, with a significant decrease in the sediment Mz and L* and an increase in the value of X lf (Figure 9). In addition, combined with climate-sea level change records, precipitation, temperature, and sporulation records from Chaohu Lake (Wang et al., 2008) are found around 8.75 ka BP, indicating the onset of a rapid temperature rise synoptic event at this time and a significant sea level rise in eastern China (Zheng, 2018), consistent with regional alluvial phase deposition under strong hydrodynamic conditions. In contrast, the δ^{18}O of NGRIP, δ^{18}O of Dongge Cave, SST, and PJJA records highlight the Younger Dryas impact hypothesis event at 11.2 ka BP, with a sharp drop in temperature, with cold-dry climate and a brief drop in sea level (Zhang et al., 2004; Praetorius et al., 2015; Ding et al., 2020; Walczak et al., 2020).

Conclusion

Detailed borehole descriptions and sedimentary stratigraphic delineation of standard boreholes in the study area were combined with OSL chronostratigraphic framework and multiple environmental proxy analysis to reconstruct the evolutionary history of the sedimentary environment in the study area since the Late Cretaceous. Influenced by the frequent oscillations of river channels and regional tectonic activity, the west bank of the study area received fluvial alluvial fan-phase deposition during the Late Tertiary and was dominated by fluvial alluvial phases after the Late Pleistocene. Since the Middle Pleistocene, the regional hydrodynamic environment has changed frequently, and the depositional environment along the east bank of the river has become complex, producing lacustrine, fluvial alluvial, and fluvial deposits.

Since the Mesozoic, the dynamical environment system in eastern China has been very complex. In the late Cretaceous, the study area experienced large-scale magmatic intrusion under the influence of the late Yanshan movement, forming diorite-porphyrite, and widely developing faults and sedimentary basins. The Neotectonic movement has been strongly manifested in the study area four times since the Late Tertiary, at the end of the Early Pleistocene or early Late Pleistocene, the end of the Middle Pleistocene, the Early to middle Late Pleistocene and the Holocene. The numerous depositional interruptions along the

river banks in the study area further demonstrate the significant role of differential sedimentation in Eastern China since the Cenozoic.

The sedimentary record in the study area is in good agreement with the geological record in the northern hemisphere and globally. The Late Cretaceous period was characterized by a significant global greenhouse climate and a high sea level phase, with a significant decrease in temperature and sea level height occurring through the Neogene period. Since the Middle Pleistocene, there have been frequent climatic fluctuations, with periods in MIS 6, 4, 3, and 2, and MIS 5b and 5d, which can be classified as periods of decreasing temperature and slow sea level rise, and periods in MIS 5a, 5c, 5e and MIS 1, when the climate was warm and wet and rapid sea level rise occurred.

Data availability statement

The raw data supporting the conclusions of this article will be made available by the authors, without undue reservation.

Author contributions

TW and LM contributed the central idea, analysed most of the data, and wrote the initial draft of the paper; HY provided the data; CZ and DM. contributed to refining the ideas, carrying out additional analyses and finalizing this paper. All authors contributed to the article and approved the submitted version.

Funding

Acknowledgments

Conflict of interest

The authors declare that the research was conducted in the absence of any commercial or financial relationships that could be construed as a potential conflict of interest.

Publisher's note

References

Aiello, G., Amato, V., Aucelli, P, P, C., Barra, D., Corrado, G., Leo, P. D., et al. (2021). Multiproxy study of cores from the garigliano plain: An insight into the late quaternary coastal evolution of central-southern Italy. *Palaeogeogr. Palaeoclimatol. Palaeoecol.* 567, 12–75.

Aitken, M. J. (1998). *An introduction to optical dating: The dating of quaternary sediments by the use of photon-stimulated luminescence* (Oxford, New York: Clarendon Press).

Bai, Y. F., Cheng, R. H., Kong, Q. Y., Tang, H. F., Cui, K. N., and Liu, P. (2007). Sedimentary paleogeography and geological background in the pukou stage of late Cretaceous period in the lower Yangtze area. *J. Jilin Univ. (Earth Sci. Edition)* 37 (04), 684–689. doi: 10.13278/j.cnki.jjuese.2007.04.005

Barrera, E., and Savin, S. M. (1999). "Evolution of late campanian-maastrichtian marine climates and oceans," in *Special paper 332: Evolution of the Cretaceous ocean-climate system*, 245–282.

Bell, L. M. (1975). *Factors influencing the sedimentary environments of the squamish river delta in southwestern British Columbia* (Doctoral dissertation, University of British Columbia).

Bornemann, A., Norris, R. D., Friedrich, O., Beckmann, B., Schouten, S., Sinninghe Damste, J. S., et al. (2008). Isotopic evidence for glaciation during cretaceous Super greenhouse. *Science* 319, 189–192.

Bouchez, J., Gaillardet, J., France-Lanord, C., Maurice, L., and Dutra-Maia, P. (2011). Grain size control of river suspended sediment geochemistry: Clues from Amazon river depth profiles. *Geochem. Geophysics Geosystems* 12 (3), 1525–2027.

Bowman, D., Korjenkov, A., Porat, N., and Czassny, B. (2004). Morphological response to quaternary deformation at an intermontane basin piedmont, the northern tien shan, kyrghyzstan. *Geomorphology* 63 (1-2), 1–24.

Cai, Z. R., Xia, B., and Wan, Z. F. (2013). The characteristics of later tectonic activities and their influence on the preservation of the Paleozoic shale gas in wuhu area, lower Yangtze platform. *J. China Coal Soc.* 38 (05), 890–895. doi: 10.13225/j.cnki.jccs.2013.05.029

Cao, K., Li, X. H., and Wang, C. S. (2006). Paleoclimate indicator and quantitative determination of paleotemperature in the Cretaceous red beds. *Acta Geologica Sichuan* 26 (04), 199–209.

Chen, Y. H. (2008). Late Cretaceous sedimentary response and paleoclimate in southeast China. *Chengdu Univ. Technol.*, 15–60.

Chen, J. (2020). "Evolutionary process of the Yangtze river," in *Evolution and water resources utilization of the Yangtze river* (Singapore: Springer), 47–122.

Cheng, H., Edwards, R. L., Sinha, A., Spötl, C., Yi, L., Chen, S., et al. (2016). The Asian monsoon over the past 640,000 years and ice age terminations. *Nature* 534 (7609), 640–646. doi: 10.1038/nature18591

Chen, H. M., and Xia, G. S. (1981). Neogene strata along the Yangtze river in anhui province. *J. Stratigr.* 5 (3), 157–164. doi: 10.19839/j.cnki.dcxzz.1981.03.001

Chen, L. Z., and Xia, G. S. (1985). Cretaceous Strata along the Yangtze river and southern anhui. *J. Stratigr.* 04), 307–313. doi: 10.19839/j.cnki.dcxzz.1985.04.011

Chen, J. M., Zhao, P., Wang, C. S., and Huang, Y. J. (2009). Modeling the East Asian climate during the late Cretaceous (80 ma). *Earth Sci. Frontier* 16 (6), 226–239.

Cheng, H., Zhang, H. W., Cai, Y. J., Shi, Z. G., Yi, L., Deng, C. L., et al. (2021). Orbital-scale Asian summer monsoon variations: Paradox and exploration. *Science China Earth Sciences* 1–16.

Chu, Q. Z., Tang, F. T., Deng, Z. H., Zhou, B., Zu, J. H., and Chen, M. H. (2008). Basic features of neotectonic movement along the lower course of Yangtze river in wuhu region. *Nonferrous Metals (Mining Section)* 60 (2), 19–23.

Cloetingh, S., and Haq, B. U. (2015). Inherited landscapes and sea level change. *Science* 347 (6220), 1258375.

Cui, C. (2017). *Late Cretaceous-Paleocene palynological stratigraphy and climatic evolution in LD17 wellof songliao basin* (Beijing: China University of Geosciences), 10–22.

Davies, A., Kemp, A, E, S., and Pike, J. (2009). Late Cretaceous seasonal ocean variability from the Arctic. *Nature* 460, 254–258. doi: 10.1038/nature08141

Ding, X. D., Zheng, L. W., Zheng, X. F., and Kao, S. J. (2020). Holocene East Asian Summer monsoon rainfall variability in Taiwan. *Front. Earth Sci.* 8, 234. doi: 10.3389/feart.2020.00234

Dong, S. W., Zhang, Y. Q., Long, C. X., Yang, Z. Y., Ji, Q., Wang, T., et al. (2007). Jurassic Tectonic Revolution in China and New Interpretation of the Yanshan Movement. *Acta Geologica Sinica* 81(11), 1449–1461.

Fan, B., Xu, S. Y., Yu, L. Z., Jiang, H., and Ran, L. H. (2006). Sedimentary phytolith assemblages and environmental evolution since Middle Holocene in Chaohu Lake. *Journal of Lake Sciences* 3, 273–279

Fang, X. Z. (2005). Geomorphic types, stratigraphic sequence division and engineering geological characteristics of wuhu area along the Yangtze plain. *Urban Geotechnical Invest. Surveying* 01), 58–60.

Feist, L., Frank, S., Bellanova, P., Laermanns, H., Cämmerer, C., Mathes-Schmidt, M., et al. (2019). The Sedimentological and Environmental Footprint of Extreme Wave Events in Boca do Rio, Algarve Coas, Portugal. *Sedimentary geology*, vol. 389. 147–160.

Folk, R. L. (1974). *Petrology of sedimentary rocks* (Austin: Hemphill Publishing Company), 1–190.

Folk, R. L., and Ward, W. C. (1957). Brazos river bar: A study in the significance of grain size parameters. *J. Sedimentary Res.* 27 (1), 3–26. doi: 10.1306/74D70646-2B21-11D7-8648000102C1865D

Foster, G. L., Royer, D. L., and Lunt, D. J. (2017). Future climate forcing potentially without precedent in the last 420 million years. *Nat. Commun.* 8 (1), 1–8. doi: 10.1038/ncomms14845

Friedrich, O., Norris, R. D., and Erbacher, J. (2012). Evolution of middle to late Cretaceous oceans-a 55 m.y. record of earth's temperature and carbon cycle. *Geology* 40 (2), 107–110. doi: 10.1130/G32701.1

Gao, Y. (2015). *Paleoclimatic evolution of the songliao basin in the late Cretaceous: Evidences from the SK-1 continental scientific drilling* (Beijing: China University of Geosciences), 12–89.

Ghandour, I. M., Al-Zubieri, A. G., Basaham, A. S., Manaa, A. A., Al-Dubai, T. A., and Jones, B. (2021). Mid-late Holocene paleoenvironmental and Sea level reconstruction on the Al lith red Sea coast, Saudi Arabia. *Front. Mar. Sci.* 23, 744. doi: 10.3389/fmars.2021.677010

Grant, K. M., Rohling, E. J., Ramsey, C. B., Cheng, H., Edwards, R. L., Florindo, F., et al. (2014). Sea-Level variability over five glacial cycles. *Nat. Commun.* 5 (1), 1–9. doi: 10.1038/ncomms6076

Guo, B. Y., Wang, Y., Zhang, B., Su, J. W., and Yang, Y. (2020). The sedimentary environment and genesis analysis of the Xiashu Formation in the Chizhou area, Anhui Province. *East China Geology* 41(01), 18–26. doi: 10.16788/j.hddz.32-1865/p.2020.01.003

Guo, J. T. (2015). *The variations and controls of Sea surface pH and pCO2 in the tropical Western pacific during the last 150 ka* (Qingdao, Shandong Province, China: The University of Chinese Academy of Sciences), 42–74.

Gu, C. J. (2005). Historical sedimentary records and environmental changes in chaohu lake. East China Normal University 7–36.

Han, B. F. (2016). *Late Cretaceous-oligocene tectonic deformation and mechanism in the oujiang sag, East China Sea continental shelf basin* (Jingzhou, Hubei Province, China: Yangtze university), 11–109.

Han, Z. Y., Li, X. S., Chen, Y. Y., and Yang, D. Y. (2009). Evolution of sedimentary enviornment of neogene gravel beds near nanjing. *Quaternary Sciences* 20 (02), 361–369.

Hansen, J., Sato, M., Russell, G., and Kharecha, P. (2013). Climate sensitivity, Sea level and atmospheric carbon dioxide. philosophical transactions of the royal society a. *Mathematical Phys. Eng. Sci.* 371 (2001), 20120294. doi: 10.1098/rsta.2012.0294

Henderson, A. L., Najman, Y., Parrish, R., BouDagher-Fadel, M., Barford, D., Garzanti, E., et al. (2010). Geology of the Cenozoic indus basin sedimentary rocks: Paleoenvironmental interpretation of sedimentation from the western himalaya during the early phases of India-Eurasia collision. *Tectonics* 29 (6), TC6015. doi: 10.1029/2009TC002651

Hou, M. J. (2005). *The magmatic activities and its deepth process of the later yanshannian granitoids in the jiangnan uplift in the area of anhui province* (Hefei, Anhui Province, China: Hefei University to Technology), 17–75.

Huang, Q., and Han, F. Q. (2019). *Introduction to climatic fluctuations and biological evolution during geological periods* (Beijing: Geology Press), 15–78.

Hu, C. S., Wu, L., and Yang, L. H. (2016). Gravel fabric and sedimentary environment of terrace gravel layers of the upper qingyijiang river at jingxian county. *Scientia Geographica Sin.* 36 (6), 951–958. doi: 10.13249/j.cnki.sgs.2016.06.019

Jiang, T., Jia, J. Z., Deng, L. J., and Wan, X. Q. (2012). Significant Climate Events in Paleogene and Their Biotic Response. *Geological Science and Technology Information* 31(3), 31–38.

Jiang, Q., He, Q., Zheng, L. G., and Hu, Y. (2019). Mineral and elemental composition of late Cretaceous dinosaur eggs in qiyunshan area, anhui province and its implication for palaeoenvironmental analysis. *Rock Mineral Anal.* 36 (04), 340–349. doi: 10.15898/j.cnki.11-2131/td.201705230086

Jiang, Y., Liu, X. M., Shi, Z. Q., Li, J. T., and Wang, Y. Y. (2021a). Review of terrestrial cretaaeous-paleogene (K/Pg) boundary in China. *J. Guilin Univ. Technol.* 41 (3), 484–496.

Jiang, Y., Wei, W., Feng, X. Y., Zhang, H., Zhu, H., and Dong, J. G. (2021b). Variation of stalagmite growth rate and its paleoclimatic significance in sanbao cave, hubei province since 640,000 years. *Carsologica Sin.* 45, 1–8.

Jin, D. S., Qiao, Y. F., Yang, L. H., and Song, X. F. (2015). A research of influence of neo-tectonic movement on alluvial rivers: Review and prospect. *Geographical Res.* 34 (3), 437–454. doi: 10.11821/dlyj201503004

Kawahata, H., Nohara, M., Aoki, K., Minoshima, K., and Gupta, L. P. (2006). Biogenic and abiogenic sedimentation in the northern East China Sea in response to sea-level change during the late pleistocene. *Global Planetary Change* 53 (1-2), 108–121. doi: 10.1016/j.gloplacha.2006.01.013

Kindler, P., and Hearty, P. J. (2022). The whale point formation: A stratigraphic record of high-frequency climate and Sea-level fluctuations in the Bahamas during marine isotope stage 5a (ca. 80 ka BP). *Sedimentary Geology* 432 (15), 106107. doi: 10.1016/j.sedgeo.2022.106107

Konert, M., and Vandenberghe, J. (1997). Comparison of laser grain size analysis with pipette and sieve analysis: A solution for the underestimation of the clay fraction. *Sedimenology* 44, 523–535. doi: 10.1046/j.1365-3091.1997.d01-38.x

Lai, Z. P. (2010). Chronology and the upper dating limit for loess samples from luochuan section in Chinese loess plateau using quartz OSL SAR protocol. *J. Asian Earth Sci.* 37 (2), 176–185. doi: 10.1016/j.jseaes.2009.08.003

Lal, R., Saini, H. S., Pant, N. C., and Mujtaba, S, A, I. (2019). Tectonics induced switching of provenance during the late quaternary aggradation of the indus river valley, ladakh, India. *Geosci. Front.* 10 (1), 285–297.

Landwehrs, J., Feulner, G., Petri, S., Sames, B., and Wagreich, M. (2021). Investigating Mesozoic Climate Trends and Sensitivities with a Large Ensemble of Climate Model Simulations. *Paleoceanography and Paleoclimatology* 36 (6), e2020PA004134.

Lea, D. W. (2000). Climate Impact of Late Quaternary Equatorial Pacific Sea Surface Temperature Variations. *Science* 289(5485), 1719–1724.

Li, Y. T. (1984). *Chinese Stratigraphy-13: The tertiary of China* (Beijing: Geology Press), 7–45.

Li, M. P. (1987). Regional geology of anhui province. *Natl. Geological Arch.*, 192–407.

Li, H. P. (2017). Neotectonic processes and their characteristics in China. *Urban Geography* 18, 109.

Lin, G. D., and Sun, H. L. (1985). *Sea Level* (Beijing: Geology Press), 33–145.

Linsley, B. K. (1996). Oxygen-isotope record of Sea level and climate variations in the sulu Sea over the past 150,000 years. *Nature* 380 (6571), 234–237.

Lisiecki, L. E., and Raymo, M. E. (2005). A pliocene-pleistocene stack of 57 globally distributed benthic δ18O records. *Paleoceanography* 20, PA1003.

Lisiecki, L. E., and Stern, J. V. (2016). Regional and global benthic δ18O stacks for the last glacial cycle. *Paleoceanography* 31 (10), 1368–1394.

Liu, X. F. (1981). Lecture of mineral particle size analysis: 1. *J. Mineralogy Petrol.* 13 (6), 104–116.

Liu, G. D. (2007). Geodynamical evolution and tectonic framework of China. *Earth Sci. Front.* 14 (3), 39–46.

Liu, X. B. (2018). *The study of magnetic properties of late Cenozoic sediments on south and north flanks of Yangtze delta: Source-sink implications for river's connection to the Sea* (Shanghai, China: East China Normal University), 15–73.

Liu, S. M., Zhang, W. G., He, Q., Li, D. J., Liu, H., and Yu, L. Z. (2010). Magnetic properties of East China Sea shelf sediments off the Yangtze estuary: Influence of provenance and particle size. *Geomorphology* 119 (3-4), 212–220.

Li, J. Y., and Zhang, J. (2003). Natural controls of sediment yield in the major rivers in China. *Periodical Ocean Univ. China (Natural Sci. Edition)* 33 (04), 565–573.

Li, R. B. (2014). *Iron oxide minerals and their palaeoclimatic significance in laterite profile in the middle to lower reaches of the yangtze river-a case study in xuancheng laterite profile.* (Beijing: China University of Geosciences) 5–115.

Li, T. F. (2020). *Organic geochemical records of paleoclimate evolution since late Pleistocene in eastern Yinchuan basin.* (Beijing: China University of Geosciences) 10–59.

Luo, W. H., Zhang, J. Z., Yang, Y. Z., Yi, C. L., and Shu, J. W. (2015). Sedimentary phytolith records of late pleistocene-middle holocene environmental evolution in Chaohu lake, Anhui province. *Acta Micropalaeontologica Sinica* 32(1), 63–74

McArthur, J. M., Howarth, R. J., and Shields, G. A. (2012). "Strontium isotope stratigraphy," in *The geologic time scale*, vol. 1. 127–144.

Miller, K. G., Kominz, M. A., Browning, J. V., Wright, J. D., Mountain, G. S., Katz, M. E., et al. (2005). The phanerozoic record of global Sea-level change. *Science* 310 (5752), 1293–1298. doi: 10.1126/science.1116412

Mills, B. J., Krause, A. J., Scotese, C. R., Hill, D. J., Shields, G. A., and Lenton, T. M. (2019). Modelling the long-term carbon cycle, atmospheric CO2, and earth surface temperature from late neoproterozoic to present day. *Gondwana Res.* 67, 172–186.

Moseley, G. E., Edwards, R. L., Lord, N. S., Spötl, C., and Cheng, H. (2021). Speleothem record of mild and wet mid-pleistocene climate in northeast Greenland. *Sci. Adv.* 7 (13), 1260. doi: 10.1126/sciadv.abe1260

Noorian, Y., Moussavi-Harami, R., Hollis, C., Reijmer, J, J, G., Mahboubi, A., and Omidpour, A. (2022). Control of climate, Sea-level fluctuations and tectonics on the pervasive dolomitization and porosity evolution of the oligo-Miocene asmari formation (Dezful embayment, SW Iran). *Sedimentary Geology* 427, 106048.

Nordt, L., Atchley, S., and Dworkin, S. (2003). "Terrestrial evidence for two greenhouse events in the latest Cretaceous," in *Geological society of America today*, vol. 13. 4–9.

O'Brien, C. L., Robinson, S. A., Pancost, R. D., Damsté, J. S. S., Schouten, S., Lunt, D. J., et al. (2017). Cretaceous Sea-Surface temperature evolution: Constraints from TEX86 and planktonic foraminiferal oxygen isotopes. *Earth-Science Rev.* 172, 224–247.

Porat, N., Zhou, L. P., Chazan, M., Noy, T., and Horowitz, L. ,. K. (1999). Dating the lower paleolith cretaceousic open-air site of holon, Israel by luminescence and ESR techniques. *Quaternary Res.* 51 (3), 328–341. doi: 10.1006/qres.1999.2036

Praetorius, S. K., Condron, A., Mix, A. C., Walczak, M. H., McKay, J. L., and Du, J. (2020). The role of northeast pacific meltwater events in deglacial climate change. *Sci. Adv.* 6 (9), 2915. doi: 10.1126/sciadv.aay2915

Praetorius, S. K., Mix, A. C., Walczak, M. H., Wolhowe, M. D., Addison, J. A., and Prahl, F. G. (2015). North pacific deglacial hypoxic events linked to abrupt ocean warming. *Nature* 527 (7578), 362–366. doi: 10.1038/nature15753

Prokoph, A., Shields, G. A., and Veizer, J. (2008). Compilation and time-series analysis of a marine carbonate δ18O, δ13C, 87Sr/86Sr and δ34S database through earth history. *Earth-Science Rev.* 87 (3-4), 113–133.

Pu, S. K., Yang, Q. H., and Pan, J. (2012). Classification and Exploration Practice of Hydrogeology in Wuhu. *Jiangsu Construction* 3, 19–23.

Qiu, D. Q. (1988). *YuXiKou banner h-50-21-D WuHu banner h-50-33-B 1/50,000 geological and mineral map bedrock geological map geological tectonic map description* (Maanshan, Anhui Province, China: Anhui Province Geological and Mineral Exploration Bureau 322 Geological Team).

Qiu, X. H. (2013). *The paleoceanographic records during the past 150 kyr B.P. in the northern part of Western pacific warm pool.* (The Institute of Oceanology: The University of Chinese Academy of Sciences), 13–104.

Qu, C. X. (2011). *Study on mesozoic intrusive rocks characteristics and distribution regularly in Yangtze river and comparative between the West hubei-Jiangxi and the east jiangsu-anhui* (Xian, Shanxi Province, China: Chang'An university), 10–101.

Qiu, Y., Sun, G. H., and Wang, Y. (2018). Subduction of the Mesozoic Pacific Ocean Plate and its Bearing on Mesozoic Deposits in The South China Sea. *Mar. Geology Front.* 34 (7), 1–8. doi: 10.16028/j.1009-2722.2018.07001

Ren, J. Y., Tamaki, K., Li, S., and Zhang, J. X. (2002). Late mesozoic and Cenozoic rifting and its dynamic setting in Eastern China and adjacent areas. *Tectonophysics* 344 (3-4), 175–205.

Shao, J. Y. (1999). Time and genesis of baishan and xiashu formations along the Yangtze river and south jiangsu. *Jiangsu geology* 23 (1), 10–16.

Singh, A., and Sinha, R. (2019). Fluvial response to climate change inferred from sediment cores from the ghaggar–hakra paleochannel in NW indo-gangetic plains. *Palaeogeogr. Palaeoclimatol. Palaeoecol.* 532 (15), 109247.

Song, W. J. (2014). *Reseach on the chronology of xiashu formation in hefei* (Beijing: China University of Geosciences), 10–35.

Song, F. M., Deng, Z. H., Ma, X. J., Zu, J. H., Chu, Q. Z., Yin, G. M., et al. (2008). Neotectonics and fault activity in the anqing-ma'anshan section of the Chang jiang river valley. *Seismology Geology* 30 (1), 100–110.

Su, Y. Y. (2007). *Analysis on land use change in wuhu city based on RS and GIS* (Wuhu, Anhui Province, China: Anhui Normal University), 15–20.

Su, J. W., Gong, J. S., Li, Y. H., Li, Y. F., Wang, Y., Dong, C. C., et al. (2019). Division of quaternary geological units based on stratigraphic architecture combination: A case study in wanjiang river economic zone. *Geological Survey China* 6 (05), 28–35. doi: 10. 19388 /j. zgdzdc. 2019. 05. 03

Sun, G. H., and Peng, G. T. (1987). A preliminary study on lithofacies paleogeography and its hydrogeological significance in Huaibei Plain since Late Pleistocene. *Hydrogeology and Engineering Geology* 1, 41–43

Tan, J., Zhang, L., Wang, C., Cao, K., and Li, X. (2020). Late Cretaceous provenance change in the jiaolai basin, East China: Implications for paleogeographic evolution of East Asia. *J. Asian Earth Sci.* 194, 104188.

Tierney, J. E., Poulsen, C. J., Montañez, I. P., Bhattacharya, T., Feng, R., Ford, H. L., et al. (2020). Past climates inform our future. *Science* 370 (6517), 3701.

Udden, J. A. (1914). Mechanical composition of clastic sediments. *Geological Soc. America Bull.* 25 (1), 655–744.

Walczak, M. H., Mix, A. C., Cowan, E. A., Fallon, S., Fifield, L. K., Alder, J. R., et al. (2020). Phasing of millennial-scale climate variability in the pacific and Atlantic oceans. *Science* 370 (6517), 716–720. doi: 10.1126/science.aba7096

Wang, H. C. (2008). *Study on the weathering indicators of sediments of the huanghe (Yellow river), changjiang (Yangtze river) and zhujiang (Pearl river) to the Sea, the comparison of the weathering intensities among the river drainage basins and their influential factors* (Qingdao, Shandong Province, China: Ocean University of China), 10–59.

Wang, Y., Fu G, H., and Zhang, Y. Z. (2007). River-sea interactive sedimentation and plain morphological evolution. *Quaternary Sci.* 27 (05), 674–689.

Wang, C., Gao, Y., Ibarra, D., Wu, H., and Wang, P. (2021). An unbroken record of climate during the age of dinosaurs. *Eos* 102, 11–60.

Wang, Y., and Ji, X. M. (2011). Environmental characteristics and changes of coastal ocean as land-ocean transitional zone of China. *Scientia Geographica Sin.* 31 (02), 129–135. doi: 10.13249/j.cnki.sgs.2011.02.129

Wang, P. C., Li, S. Z., Liu, X., Yu, S., Liu, H., Suo, Y. H., et al. (2012). Yanshanian fold-thrust tectonics and dynamics in the middle-lower Yangtze river area, China. *Acta Petrologica Sin.* 28 (10), 3418–3430.

Wang, Y., Huang, C., Sun, B., Quan, C., Wu, J., and Lin, Z. (2014). Paleo-CO_2 variation trends and the Cretaceous greenhouse climate. *Earth-Science Reviews* 129, 136–147.

Wang, X. Y., Mo, D. W., Wu, L., Zhang, G. S., Xiao, X. Y., and Han, W. G. (2008). Pollen record from chaohu lake in the lower reaches of the changjiang river and environmental changes since 9870 Cal·aB·P. *Quaternary Sci.* 28 (4), 649–658.

Wang, P., Suo, Y., Cao, X., Zhu, J., Liu, B., Wang, G. Z., et al. (2022). Late Cretaceous-Cenozoic cooling of the southern lower Yangtze river area: A response to subduction of the izanagi and pacific plates. *Gondwana Res.* 102, 31–45.

Wei, Z. X. (2003). *Quaternary environmental evolution in Eastern Yangtze delta: Coupling of neotectonic movement, paleoclimate and Sea-level fluctuation* (Shanghai, China: East China Normal University), 13–112.

Wentworth, C. K. (1922). A scale of grade and class terms for clastic sediments. *J. Geology* 30 (5), 377–392.

Westerhold, T., Marwan, N., Drury, A. J., Liebrand, D., Agnini, C., Anagnostou, E., et al. (2020). An astronomically dated record of Earth's climate and its predictability over the last 66 million years. *Science* 369(6509), 1383–1387.

Wintle, A. G. (2008). Luminescence dating of quaternary sediments-introduction. *Boreas* 37 (4), 469–470.

Wuhu Local Records Compilation Committee (WLRCC) (1993). *Records of wuhu city* Vol. Vol.1 (Beijing: Social Sciences Academic Press), 67–68.

Wu, H. D., Lu, Y. C., Li, S. T., Xie, X. N., Li, L. P., Zhou, P., et al. (1998). Tertiary sequence stratigraphic framework and Sea-level changes in the East China Sea shelf basin. *Earth Sci.* 23 (1), 13–20.

Wu, L. L., Mei, L. F., Paton, D. A., Liu, Y. S., Guo, P. Y., Shen, C. B., et al. (2020). Late Cretaceous-Cenozoic intraplate extension and tectonic transitions in Eastern China: Implications for intraplate geodynamic origin. *Mar. Petroleum Geology* 117, 104379.

Xiang, F., Song, J. C., Luo, L., and Tian, X. (2009). Distribution characteristics and climate significance of continental special deposits in the early Cretaceous. *Earth Sci. Front.* 16 (05), 48–62.

Xiong, S. F., Ding, Z. L., and Liu, D. S. (1998). The problems and progress in the studies of mechanisms for quaternary climate changes. *Adv. Earth Sci.* 13 (03), 50–57.

Xu, B. L. (2008). *Study on paleoclimate of late mesozoic in the north China* (Chengdu, Sichuan Province, China: Chengdu University of Technology), 10–82.

Xu, X., and Gao, S. L. (2015). The structure and formation of the Cenozoic fault basin in the lower Yangtze region. *Earth Sci. Front.* 22 (06), 148–166. doi: 10.13745/j.esf.2015.06.011

Xu, X., Liang, C., and Xu, Y. (2021). Kinematic analysis of fault-slip data in the nanling tectonic belt and Cretaceous to paleogene tectonic evolution of the central south China block. *J. Asian Earth Sci.* 221, 104951.

Xu, X. L., Li, H. W., Tang, L. J., Lai, Z. P., Xu, G. J., Zhang, X. H., et al. (2020). Chronology of a Holocene core from the pearl river delta in southern China. *Front. Earth Sci.* 8, 262.

Xu, W., Wang, Y. S., Tong, J. S., Chen, X. Q., and Xing, R. H. (1999). The features of neotectonic movement in hefei and East beyond. *Geology Anhui* 9 (4), 250–254.

Xu, X., Zhu, X. Y., Shan, X. P., Xiao, M. C., Sun, L. P., and Gao, S. L. (2018). Structure and sedimentary characteristics of the meso-Cenozoic basin groups along the Yangtze river in the lower Yangtze region. *Petroleum Geology Experiment* 40 (03), 303–314. doi: 10.11781/sysydz201803303

Xu, X., Zhang, S. W., and Zhou, S. (1987). A Preliminary Study on Vegetation, Climate and Environment in Wuhu-Jiangyin Region for 30,000 Years. *Journal of Nanjing University (Natural Science)* 3, 556–577.

Yan, W., Chen, Z., Wang, Y. Q., and Chen, M. H. (2000). Mineralogical characteristics and mineralsedimentary sequences of core NS93-5 from south China ses. *Acta Mineralogica Sin.* 20 (02), 143–149.

Yang, Y. (2008). *The sedimentary environments and climatic significance of xiashu loess in chaohu area* (Wuhan: China University of Geosciences), 7–52.

Yan, Y. S., and Huang, Z. Q. (1999). Quaternary sedmentaion and paleoenvironmental changes of the qingyi river area and the shuiyang river areain the southern anhui province. *Journal of Jiangsu Normal University* 1, 58–64.

Yan, L., Cao, H., Wang, X. Y., Zhang, D. P., Wang, W. B., and Guo, X. L. (2022). Polycyclic aromatic hydrocarbons in the upper Cretaceous lacustrine deposits from the songliao basin (NE china): Implications for wildfires and paleoclimate. *Palaeogeography, Palaeoclimatology, Palaeoecology* 600, 31–182. doi: 10.1016/j.palaeo.2022.111083

Yang, D. Y., and Li, X. S. (1998). Geomorphologic masks and basic feature of neotectonic movement in the Eastern China. *Quaternary Sci.* 03, 249–255.

Yang, H. B., Tian, X. B., Bai, Z. M., and Zhang, Z. J.. (2016). Discussion on the relationship between pan pacific plate movement and mesozoic geological evolution of Eastern Chinese continent. *J. Jilin University (Earth Sci. Edition)* 46 (3), 781–797. doi: 1 0.13278/j.cnki.jjuese.201603114

Yang, L. R., and Xie, Z. R. (1984). Sea-Level changes along the East coast of China over the last 20000 years. *Oceanologia Limnologia Sin.* 15 (1), 1–13.

Yang, J. L., Yuan, H. F., Hu, Y. Z., and Wang, F. (2022). Significance of sedimentary provenance reconstruction based on borehole records of the north China plain for the evolution of the yellow river. *Geomorphology* 401 (15), 108077.

Yan, Y. S., and Huang, Z. Q. (1991). Quaternary sedimentation and environmental change in qingyijiang and shuiyangjiang areas of southern Anhui Province. *J. Xuzhou Normal Univ. (Natural Sci. Edition)* 01, 58–64.

Yao, J. (2014). *Climatic indicators and sedimentary environment studies inferred from transgressive and regressive sediments of core LZ908, south bohai Sea* (Qingdao, Shandong Province, China: Institute of Oceanology, Chinese Academy of Sciences), 13–111.

Yuan, D. X., Cheng, H., Edwards, R. L., Dykoski, C. A., Kelly, M. J., Zhang, M. L., et al. (2004). Timing, duration, and transitions of the last interglacial Asian monsoon. *Science* 304 (5670), 575–578.

Yuan, H. Q., Wang, L., Yu, Y. H., Zhang, D. J., Xu, F. M., and Liu, H. T. (2019). Review of sedimentary grain size analysis methods. *J. Jilin Univ. (Earth Sci. Edition)* 49 (2), 380–393. doi: 10.13278/j.cnki.jjuese.20180055

Yu, Z. J., and Huang, D. C. (1996a). Formation environment of net-veined laterite and xiashu loess and their ages in the Ares along the Yangtze river, Anhui Province. *Geology Anhui* 6 (03), 48–56.

Yu, Z. J., and Huang, D. C. (1996b). The pliocene-Holocene petrostratigarphic units and their ages in the huaibei plain, anhui. *Geology Anhui* 6 (02), 21–29.

Yu, Z. J., and Peng, Y. H. (2008). Quaternary lithostratigraphic sequence in anhui province. *Acta Geologica Sin.* 82 (02), 254–261.

Yu, Y., and Xu, X. S. (2009). *Cretaceous Alkal-i rich magmatism in the middle and lower reaches of the Yangtze river earth* Vol. 34 (Beijing, China: Science-Journal of China University of Geosciences), 1-32.

Zhang, L. M. (2016). *Paleoclimatic evolution and mechanism of the mass extinction during the K-Pg boundary: Evidences from several terrestrial basins in East China* (Beijing: China University of Geosciences), 10–43.

Zhang, R. H. (2011). *The Yangtze river delta: Holocene sedimentary environmental evolution and implications of East Asian summer-monsoon inferred from sediment records* (East China Normal University), 16–134.

Zhang, W. W. (2013). *Study on paleoclimate and environment changes in northern of jiangsu basin since 360,000 years* (Nanjing, Jiangsu Province, China: Nanjing Normal University), 7–61.

Zhang, M. Z. (2014). *Late mesozoic environment and ecology evolution based on palynological records from central East Asia* (Lanzhou University), 12–136.

Zhang, M. L., Cheng, H., Lin, Y. S., Gu, J. M., Zhang, H. L., Tu, L. L., et al. (2004). High resolution paleoclimatic environment records from a stalagmite of dongge cave since 15000a in libo, guizhou province, China. *Geochimica* 33 (1), 65–74.

Zhang, Z. Y., He, W. H., Wei, Y., Ke, X., and Luo, M. S. (2014). Evolution of mesozoic sedimentary basins in the lower Yangtze. *Earth Science-Journal China Univ. Geosciences* 39 (8), 1017–1034.

Zhang, L. T., and Huang, H. (1989). The characteristics and evolution of meso-Cenozoic continental down-faulted basins in auhui province. *Regtonal Geology China* 2, 129–137.

Zhang, S., Hu, X., Han, Z., Li, J., and Garzanti, E. (2018a). Climatic and tectonic controls on Cretaceous-palaeogene Sea-level changes recorded in the tarim epicontinental Sea. *Palaeogeogr. Palaeoclimatol. Palaeoecol.* 501, 92–110. doi: 10.1016/j.palaeo.2018.04.008

Zhang, X. B., Liu, Y., Wang, S. J., Liu, W. M., and Xue, W. X. (2018b). On the chronology of the yellow rivers and the Yangtze rivers. *Mountain Res.* 36 (05), 661–668. doi: 10.16089/j.cnki.1008-2786.000362

Zhang, S. G., Zhang, Y. B., and Yan, H. J. (2015). Introduction to the stratigraphic chart of China. *J. Stratigr.* 39 (04), 359–366.

Zhang, Y. L., Wang, K. F., Wang, Y. Y., Wang, J. W., Wang, R., Wang, C, , F., et al. (1986). Early Tertiary sporulation assemblages and their geological significance in the Nanling Basin, Anhui. *Oil and Gas Geology* 1, 75–114.

Zhao, X. W. (1992). *Introduction to Paleoclimatology*. (Beijing: Geology Press) 15–70.

Zhao, D. B. (2017). *Sedimentarv evolution in northern Okinawa Trough and their environmental response since the last 400 ka.* (The Institute of Oceanology: Chinese Academy of Sciences) 14–128.

Zheng, B. (2018). *Holocene Vegetation and climate changes and provenance input based om geochemical records from the mud shelf sediments of the East China Sea* (Nanjing, Jiangsu Province, China: Naijing University), 12–34.

Zheng, C. H. (2019). *Evaluation of crustal stability in the anhui section of the tanlu fault zone* (Hefei, Anhui Province, China: Hefei University of Technology), 19–47.

Zheng, Y. F., Xiao, W. J., and Zhao, G. H. (2013). Introduction to tectonics of China. *Gondwana Res.* (Nanjing, Jiangsu Province, China) 23 (4), 1189–1206. doi: 10.1016/j.gr.2012.10.001

Zhong, L. (2010). *The research of late pleistocene glaciation climate and tectonic movement coupling relations of in eastern China*. Liaoning Normal University 4–32

Zhou, Y. C., and Chen, Y. C. (1992). A discussion on the indosinian movement in the tongling and fangchang areas. *Geology Anhui* 02 (03), 71–78.

Zhu, C. G. (2020). *Climate and ocean circulation response to the atmospheric CO_2 and paleogeography changes during the paleogene* (Wuhan, Hubei Province, China: China University of Geosciences), 11–108.

Zhuang, L. H. (2002). *Late Quaternary paleoenvironmental evolution and sea-level change on the Yellow East Sea shelf* (The Institute of Oceanology: Chinese Academy of Sciences), 8-60.

Zhu, J. J., Wang, Q., Liang, J. S., Wang, H., Tian, B., and Hao, L. W. (2012). Cenozoic Geological structure and tectonic evolution of southern East China Sea shelf basin. *Natural Gas Geosci.* 23 (2), 222–229.

Zhu, C., Zheng, C. G., Ma, C. M., Yang, X. X., Gao, X. Z., Wang, H. M., et al. (2003). A new understanding of the high Sea level in the Yangtze river delta and ningshao plain in the past ten thousand years. *Chin. Sci. Bull.* 48 (23), 2428–2438.